JOURNAL OF GEOPHYSICAL RESEARCH, VOL. 115, G01004, doi:10.1029/2009JG001163, 2010

A modeling investigation of canopy-air oxygen isotopic exchange of water vapor and carbon dioxide in a soybean field

Wei Xiao,[1,2] Xuhui Lee,[3] Timothy J. Griffis,[4] Kyounghee Kim,[3] Lisa R. Welp,[5] and Qiang Yu[2,6]

Received 27 September 2009; accepted 9 October 2009; published 16 January 2010.

[1] The oxygen isotopes of CO_2 and H_2O (^{18}O-CO_2 and ^{18}O-H_2O) provide unique information regarding the contribution of terrestrial vegetation to the global CO_2 and H_2O cycles. In this paper, a simple isotopic land surface model was used to investigate processes controlling the isotopic exchange of ^{18}O-H_2O and ^{18}O-CO_2 between a soybean ecosystem and the atmosphere. We included in a standard land surface model a nonsteady state theory of leaf water isotopic composition, a canopy kinetic fractionation factor, and a big-leaf parameterization of the ^{18}O-CO_2 isoforcing on the atmosphere. Our model simulations showed that the Péclet effect was less important than the nonsteady state effect on the temporal dynamics of the water isotopic exchange. The model reproduced the highly significant and negative correlation between relative humidity and the ecosystem-scale ^{18}O-CO_2 isoforcing measured with eddy covariance. But the model-predicted isoforcing was biased high in comparison to the observations. Model sensitivity analysis suggested that the CO_2 hydration efficiency must have been much lower in the leaves of soybean in field conditions than previously reported. Understanding environmental controls on the hydration efficiency and the scaling from the leaf to the canopy represents an area in need of more research.

Citation: Xiao, W., X. Lee, T. J. Griffis, K. Kim, L. R. Welp, and Q. Yu (2010), A modeling investigation of canopy-air oxygen isotopic exchange of water vapor and carbon dioxide in a soybean field, *J. Geophys. Res.*, *115*, G01004, doi:10.1029/2009JG001163.

1. Introduction

[2] Studying the $^{18}O/^{16}O$ ratio in CO_2 and H_2O can provide constraints on the water and carbon exchange processes between the land and the atmosphere. The lower vapor pressure and diffusion rate of $H_2^{18}O$ molecules compared to $H_2^{16}O$ cause $H_2^{18}O$ to accumulate in the leaf water during transpiration. Oxygen atoms exchange between the CO_2 and H_2O molecules in a hydration reaction catalyzed by carbonic anhydrase. Consequently, those CO_2 molecules that diffuse from the leaf back to the atmosphere carry the isotopic signal of the leaf water [*Farquhar et al.*, 1993]. Understanding the fractionation processes and the mechanisms controlling land-atmosphere ^{18}O-CO_2 and ^{18}O-H_2O exchange can help to resolve a number of important questions related to global carbon and water cycles. At present, we lack the capacity to interpret long-term changes in the isotopic composition of the atmosphere and the ability to decipher if these changes are related to climate variability, changes in land use, or other anthropogenic activities.

[3] Land surface models (LSMs) are a powerful tool for integrating the isotopic fractionation processes with CO_2 and H_2O exchange in terrestrial ecosystems. *Cuntz et al.* [2003a, 2003b] and *Hoffmann et al.* [2004] used LSMs to simulate ^{18}O-H_2O and ^{18}O-CO_2 budgets on the global scale. *Farquhar et al.* [1993] calculated the global ^{18}O-CO_2 composition to investigate the oxygen fractionation mechanism by using the observed meteorology, and highlighted the different effects on atmospheric ^{18}O-CO_2 composition of terrestrial and oceanic fluxes. *Gillon and Yakir* [2001] used the SiB2 model to calculate a global mean value for the extent of ^{18}O equilibrium between CO_2 and leaf water and quantify large differences in carbonic anhydrase activity among major plant groups. *Riley et al.* [2002, 2003] developed a two-leaf isotopic model to simulate ^{18}O-H_2O and ^{18}O-CO_2 exchange at the ecosystem scale. So far, the validation of LSMs for the ^{18}O-CO_2 flux have been inhibited by the lack of high-resolution isotopic data under field conditions [*McDowell et al.*, 2008].

[4] This paper aims to investigate, using a simple isotopic LSM (SiLSM), the isotopic exchange of ^{18}O-H_2O and ^{18}O-CO_2 between a soybean ecosystem and the atmosphere.

[1]Key Laboratory of Meteorological Disaster of Ministry of Education, College of Applied Meteorology, Nanjing University of Information Science and Technology, Nanjing, China.
[2]Institute of Geographical Sciences and Natural Resources Research, Chinese Academy of Sciences, Beijing, China.
[3]School of Forestry and Environmental Studies, Yale University, New Haven, Connecticut, USA.
[4]Department of Soil, Water, and Climate, University of Minnesota, Saint Paul, Minnesota, USA.
[5]Scripps Institution of Oceanography, University of California, San Diego, La Jolla, California, USA.
[6]Plant Functional Biology and Climate Change Cluster, Department of Environmental Sciences, University of Technology Sydney, Broadway, New South Wales, Australia.

0148-0227/10/2009JG001163$09.00

The model has integrated the latest advances, both experimental and theoretical, on fractionation processes controlling the isotopic exchange. One unique feature of our work is that key isotopic variables were measured at a high temporal resolution to drive and validate the isotopic LSM. These data were obtained in a field experiment where the isotopic fluxes of ^{18}O-CO_2 and ^{18}O-H_2O were measured with eddy covariance and flux-gradient methods, along with supporting measurements of ^{18}O-H_2O in ecosystem water pools, $^{18}O/^{16}O$ ratio in atmospheric CO_2 and micrometeorological variables [*Griffis et al.*, 2005b, 2008; *Lee et al.*, 2005; *Welp et al.*, 2008]. Our strategy is to constrain the standard flux parameterizations with the field observations but keep to a minimum the tuning of parameters related to the isotopic processes. The disagreement between the calculated and observed isotopic fluxes should therefore help us identify deficiencies in the current knowledge of the isotopic exchange.

[5] Our SiLSM adopts the system of equations of *Farquhar and Cernusak* [2005] for predicting the ^{18}O-H_2O composition of leaf water ($\delta^w_{L,e}$) in nonsteady state. Modeling $\delta^w_{L,e}$ is a crucial part of isotopic LSMs because $\delta^w_{L,e}$ plays a major role in the ^{18}O-CO_2 flux from the ecosystem to atmosphere [*Farquhar et al.*, 1993]. An improved understanding of $\delta^w_{L,e}$ and the associated canopy ^{18}O-CO_2 flux should benefit researchers who wish to partition the net CO_2 flux into gross photosynthesis and respiration components [*Ogee et al.*, 2004; *Yakir and Wang*, 1996], reconstruct palaeoclimate with plant materials [*Cullen et al.*, 2008; *Epstein and Yapp*, 1977; *Gray and Thompson*, 1976; *Libby et al.*, 1976; *Roden et al.*, 2000], and estimate the Dole effect [*Bender et al.*, 1994; *Hoffmann et al.*, 2004]. *Dongmann et al.* [1974] made the first attempt at calculating the isotopic composition of leaf water in nonsteady state using the Craig-Gordon model on the assumption that leaf water is evenly enriched in ^{18}O. The study of *Farquhar and Cernusak* [2005] accounted for both the nonsteady state effects [*Wang and Yakir*, 1995] and progressive enrichment of ^{18}O from the xylem to the site of evaporation according to the Péclet effect [*Farquhar and Lloyd*, 1993]. The in situ measurement of the isotopic composition of canopy transpiration [*Welp et al.*, 2008] and the high-frequency measurement of the bulk leaf water δ [*Farquhar and Cernusak*, 2005] suggest the necessity to consider nonsteady state and the Péclet effect in field conditions. The original set of equations of *Farquhar and Cernusak* [2005] are developed for the leaf scale. Here we extend these concepts to the canopy scale.

[6] Kinetic fractionation is another crucial factor controlling the isotopic exchange between ecosystems and the atmosphere. In leaf-scale studies, kinetic fractionation is regarded as a function of the kinetic factors associated with the stomatal resistance and the leaf boundary layer resistance [*Dongmann et al.*, 1974; *Farquhar and Lloyd*, 1993; *Flanagan et al.*, 1991]. At the canopy scale the role of turbulent diffusion is not treated in a consistent manner [*Ciais et al.*, 1997; *Cuntz et al.*, 2003a; *Dongmann et al.*, 1974; *Farquhar et al.*, 1993; *Hoffmann et al.*, 2004; *Riley et al.*, 2002]. The first direct isotopic flux measurements mentioned above have confirmed the need to consider air turbulent diffusion when calculating the isoforcing of ^{18}O-CO_2 and the enrichment of leaf water in ^{18}O. Here, the canopy-scale fractionation factors and the big-leaf isoforcing parameterization developed by *Lee et al.* [2009] have been integrated into SiLSM.

[7] Another goal of this study is to perform model sensitivity analyses to identify potential sources of error for isotope LSM parameterizations and variables that exert large control on the isotopic fluxes. This goal is motivated by the fact that the observational data alone cannot disentangle the complex role of various fractionation processes. Specifically, we will address three issues including: (1) the importance of energy balance closure in model studies; (2) the sensitivity of canopy ^{18}O-CO_2 exchange to the CO_2 hydration extent within the leaves and soil; (3) the effects of elevated CO_2 concentration, wind speed, humidity, temperature and soil moisture on the isotopic fluxes from the ecosystem to the atmosphere.

2. Experimental Methods

[8] The field measurements were taken in 2006 at the University of Minnesota's Rosemount Research and Outreach Center, about 25 km south of St. Paul, MN. The experimental site is part of the AmeriFlux network and managed in a corn-soybean rotation typical of the Upper Midwest. This experiment was conducted during the soybean (C3) phase of the rotation. Detailed information about this site and instrumentations can be found in other papers [*Baker and Griffis*, 2005; *Griffis et al.*, 2005a, 2005b, 2007, 2008; *Welp et al.*, 2008]. Soybeans were planted on 24 May (day of year or DOY 144), with the maximum LAI of 8.15 reached around 3 August (DOY 215). The maximum plant height was about 1 m.

[9] Isotopic measurements of CO_2 and water vapor were made with three tunable diode laser (TDL) analyzers (model TGA100A, Campbell Scientific, Inc., Logan, Utah). One analyzer was used to measure the isotope ratio of water vapor (δ^w_a) at two heights above the canopy. The hourly $^{18}O/^{16}O$ isotope ratio of evapotranspiration (δ^w_{ET}) was obtained from the flux-gradient approach [*Welp et al.*, 2008]. The second TDL analyzer, also deployed in the flux-gradient mode, measured the $^{18}O/^{16}O$ and $^{13}C/^{12}C$ isotope ratio of atmospheric CO_2 at two heights over the canopy. From 18 July to 20 September, a third TDL analyzer was used in the closed-path eddy covariance (EC-TDL) mode to measure the covariance $w'\delta'$, which is a direct measure of the $C^{18}O^{16}O$ isoforcing [*Griffis et al.*, 2008]. The TDL analyzers were installed at the north edge of the field and the data were sensitive to wind direction. The $^{18}O/^{16}O$ ratios in atmospheric water vapor and CO_2 are among the driving variables of SiLSM and the measurements of the ^{18}O-CO_2 isoforcing and δ^w_{ET} were used to evaluate the performance of the model.

[10] Supporting measurements consisted of standard micrometeorological variables and the ^{18}O-H_2O content of ecosystem water pools. We measured the eddy fluxes of heat, water vapor, momentum and standard micrometeorological variables (air temperature and humidity, canopy temperature, wind speed and direction, soil temperature and moisture). We sampled the ^{18}O-H_2O content of ecosystem water pools at varying time intervals: leaf samples were collected daily (at midday), and stem and 10 cm soil samples were collected every week, except during a 3 day intensive period (DOY 208–210) when leaf samples were collected every 3 h, stem and soil (0, 5, 10 cm depth) every 6 h, and 20 cm soil once per day.

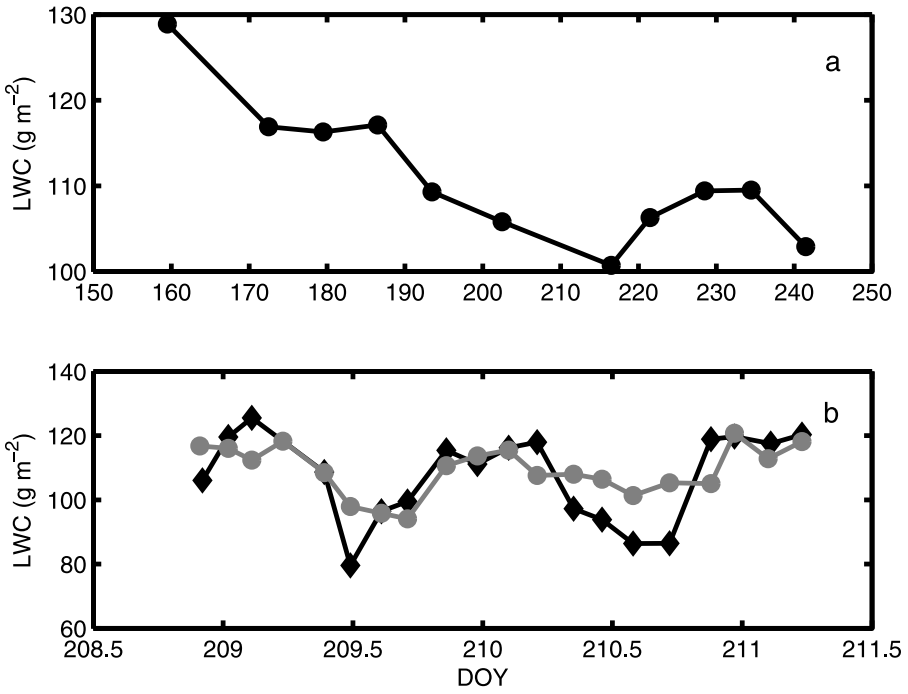

Figure 1. Time variations of leaf water content (in units of g of water per m^2 of leaf area). (a) Seasonal variation measured at midday; (b) Diurnal variation in the upper canopy layer (circles) and lower canopy layer (diamonds) during the intensive measurement period.

[11] Leaf water content is a critical variable in determining the leaf water δ in nonsteady state. It was measured at midday once every week from DOY 159 to 241 (Figure 1a). Leaf water content was 128.9 g m^{-2} (mass of water per unit leaf area) at the beginning of the growing season and declined to 100.7 g m^{-2} before leaf senescence, with a mean value 111.2 g m^{-2}. During the intensive period, it was measured every 3 h at the top and bottom of the canopy. The magnitude of diurnal leaf water content variation was bigger at the bottom of the canopy than at the top (Figure 1b). For the bottom leaves, it varied from 79.6 g m^{-2} around midday to 125.5 g m^{-2} at night, with a mean value 107.2 g m^{-2}. For the top leaves, it varied from 94.1 g m^{-2} around midday to 120.7 g m^{-2} at night, with a mean value 109.2 g m^{-2}.

3. Model Description

3.1. Model Structure

[12] A detailed description of SiLSM is provided in Appendices A–C. Briefly, the model consists of three submodels (Figure 2). A big leaf parameterization of the ^{18}O-CO_2 isoforcing on the atmosphere derived by *Lee et al.* [2009], the central part of the model, calculates ecosystem ^{18}O-CO_2 isoforcing and its canopy and soil components as the final outputs (Appendix A). Here the isoforcing is represented by the covariance of the vertical velocity and the ^{18}O-CO_2 composition in air, $w'\delta'$ (in units of ‰ m s^{-1}). *Lee et al.* [2009] showed that this covariance is the proper lower boundary condition for evaluating atmospheric ^{18}O-CO_2 budget. For historical reasons, we also use the quantity C_a ($w'\delta'$), termed as eddy isoforcing, which carries the dimensions of isoflux (μmol m^{-2} s^{-1} ‰). The driving variables of this submodel are the concentration (C_a) and ^{18}O isotopic composition (δ_a^c) of the atmosphere CO_2, both measured at a reference height of 3.0 m above the ground. A complete list of symbol definitions is provided in the notation section.

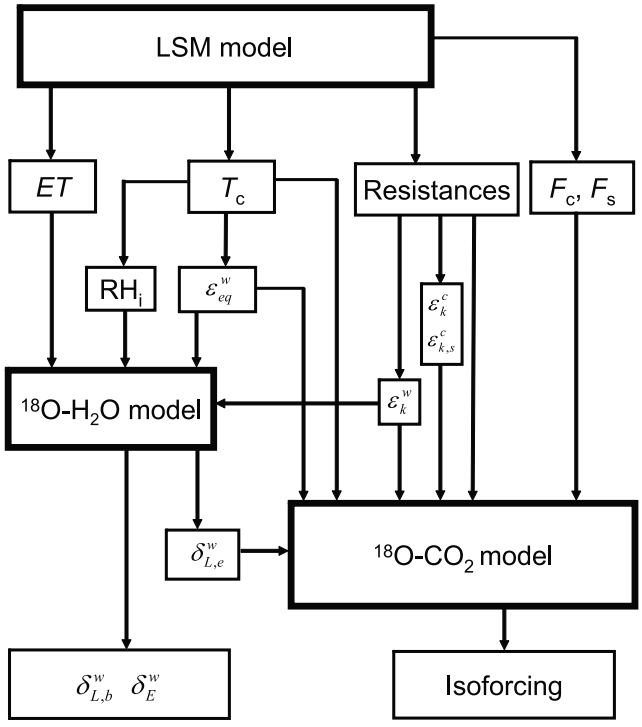

Figure 2. Relationship between SiLSM model components. Symbols are defined in the notation section.

[13] The second submodel deals with ^{18}O in leaf water. Several studies show that leaf water is usually in nonsteady state in a diurnally varying humidity regime, wherein the isotopic compositions of the source water and the transpiration water are not the same [*Cernusak et al.*, 2002, 2005; *Harwood et al.*, 1998; *Lee et al.*, 2009; *Wang and Yakir*, 1995]. A system of equations developed by *Farquhar and Cernusak* [2005] was employed to determine a critical but nonmeasurable variable, the ^{18}O-H_2O composition at the evaporative site $\delta^w_{L,e}$, and predict the ^{18}O-H_2O composition of bulk leaf water ($\delta^w_{L,b}$) and evapotranspiration (δ^w_{ET}) for comparison with the measurement (Appendix B).

[14] The canopy and soil CO_2 flux, evapotranspiration rate, canopy temperature and resistance terms were computed using the big-leaf LSM of *Ronda et al.* [2001], with three important changes (Appendix C). This LSM was selected for several reasons. First, because it is a big leaf model, it can be easily interfaced with the big leaf version of the *Farquhar and Cernusak* [2005] model for the leaf water isotope and the big-leaf isoforcing parameterization we have recently developed [*Lee et al.*, 2009]. Second, this LSM was recently coupled to the NCAR's large eddy simulation model (LES) [*Huang et al.*, 2008]. Efforts are underway to expand the LES model to simulate the carbon and water isotopic budgets in the atmospheric boundary layer. Finally, the LSM considers the nonlinear response of plant physiology to light penetration inside the canopy, which is usually ignored in other big-leaf LSMs. Its treatment of the response is crude in comparison to the two-leaf sunlit and shade model of *Riley et al.* [2002] and the multilayer models of *Baldocchi and Bowling* [2003] and *Ogee et al.* [2007]. However, the choice of the simple LSM is justified by the fact that we did not have detailed micrometeorological measurements inside the canopy to verify the predictions of the multilayer schemes. Also it is not straightforward to implement the Farquhar's nonsteady state method in the two-leaf model because it requires tracking of the leaf water ^{18}O budget in a fix number of leaves whereas in a two-leaf scheme the fractions of sunlit and shade leaves change through the course of the day [*Riley et al.*, 2002, 2003; *Wang and Leuning*, 1998].

[15] Soil variables, except for the soil CO_2 flux, were not parameterized; instead they were provided by the measurement. In this regard, our model is suitable for the intended purpose of diagnostic analysis but is less useful for prognostic prediction.

[16] The ^{18}O-CO_2 composition was referenced to the Vienna Pee Dee Belemnite (VPDB) scale, and ^{18}O-H_2O composition was referenced to the Vienna Standard Mean Ocean Water (VSMOW).

3.2. Input Data

[17] The SiLSM model was driven by field observations of (1) plant variables including leaf area index (LAI), leaf water content per unit ground area (W) and canopy height (h), (2) micrometeorological variables including air temperature (T_a), soil temperature (T_s), relative humidity of air (RH), soil moisture content (θ), solar radiation (R_S), sky long-wave radiation (R_L), atmospheric CO_2 concentration (C_a), wind speed (u_m) and friction velocity (u_*), and (3) ^{18}O composition of atmospheric CO_2 (δ^c_a) and H_2O vapor (δ^w_a) measured at the reference height, and the ^{18}O-H_2O composition of xylem water (δ^w_x) and soil water (δ^w_s). Here T_s and θ were measured at 10 cm depth of soil, and all other variables were measured at the reference height of 3.0 m above the ground.

[18] Not all driving variables were measured at the 30 min time step of the SiLSM model. Linear interpolation was carried out for LAI, h, δ^w_x and δ^w_s from the discrete measurements described in section 2. The W time series was constructed by superimposing the diurnal variation measured during the intensive campaign (Figure 1b) to the seasonal trend of the weekly data (Figure 1a) and multiplying by LAI.

3.3. Model Parameterization

[19] The lack of energy balance closure in eddy covariance measurement introduced a dilemma for the LSM model validation since the model was based on the principle of energy budget conservation. The sum of the measured latent heat flux (LE), sensible heat flux (H) and soil heat flux (G) accounted for 69% of the net radiation (R_n), with heat storage in the canopy layer being ignored. Such imbalance is typical of experiments over low vegetation [*Foken*, 2008]. In another synthesis study, *Wilson et al.* [2002] reported an average 20% imbalance among the FluxNet sites. To satisfy energy conservation, we adjusted the LE and H measurement by forcing energy balance closure with the assumption that the available energy ($R_n - G$) and the Bowen ratio H/LE were accurately measured [*Blanken et al.*, 1997]. Other modelers have also reported the need to force energy balance closure for model parameterization and validation [*Aranibar et al.*, 2006].

[20] The LSM submodel contains four tunable parameters. Two of them (b_1 and b_2) describe the dependence of photosynthesis on soil moisture (equation (C15)) and the other two appear in the stomatal resistance parameterization (the vapor pressure deficit constant D_0 and CO_2 concentration constant a_1 in equation (11) of *Ronda et al.* [2001]). Since no leaf-scale ecophysiological measurements were available to constrain these parameters, they were tuned with the ecosystem-scale data. First, D_0 and a_1 were tuned by a nonlinear least squares method so that the predicted net ecosystem CO_2 flux (F_N) was optimized to match the observed F_N. Next, b_1 and b_2 were tuned to optimize the prediction of LE. The optimized values were $D_0 = 0.44$ kPa, and $a_1 = 16.2$, $b_1 = -5.8$ and $b_2 = -24.9$ for $\theta \leq 0.21$, $b_1 = -1.5$ and $b_2 = -24.9$ for $\theta > 0.21$.

[21] The ^{18}O-H_2O submodel contains one free parameter, L_{eff}, the scaled effective "radial" length in the Péclet number. It was optimized with the ^{18}O composition of the bulk leaf water ($\delta^w_{L,b}$) measured in midday hours. The optimized value of L_{eff} was less than 0.01 mm. This is much lower than the values of 6.25 mm in *Phaseolus vulgaris* and 13.5 mm in *Ricinus communis* found by other authors [*Barbour and Farquhar*, 2000; *Barbour et al.*, 2000; *Cernusak et al.*, 2003; *Flanagan et al.*, 1994]. *Welp et al.* [2008] obtained a L_{eff} value of 20 mm by tuning the Farquhar and Cernusak predicted $\delta^w_{L,b}$ against the measured $\delta^w_{L,b}$, using kinetic fractionation factors that ignore aerodynamic diffusion. The extremely low L_{eff} suggests that the Péclet effect was negligible.

[22] The ^{18}O-CO_2 isoforcing submodel contains two free parameters, θ_{eq} and $\theta_{eq,s}$. We used the value of 0.75 for soybean θ_{eq} reported by *Gillon and Yakir* [2000] and set $\theta_{eq,s}$ to 1. No tuning of these parameters was made, so the disagreement between the calculated and observed isoforcing helps us identify deficiencies in the current knowledge of the isotopic exchange.

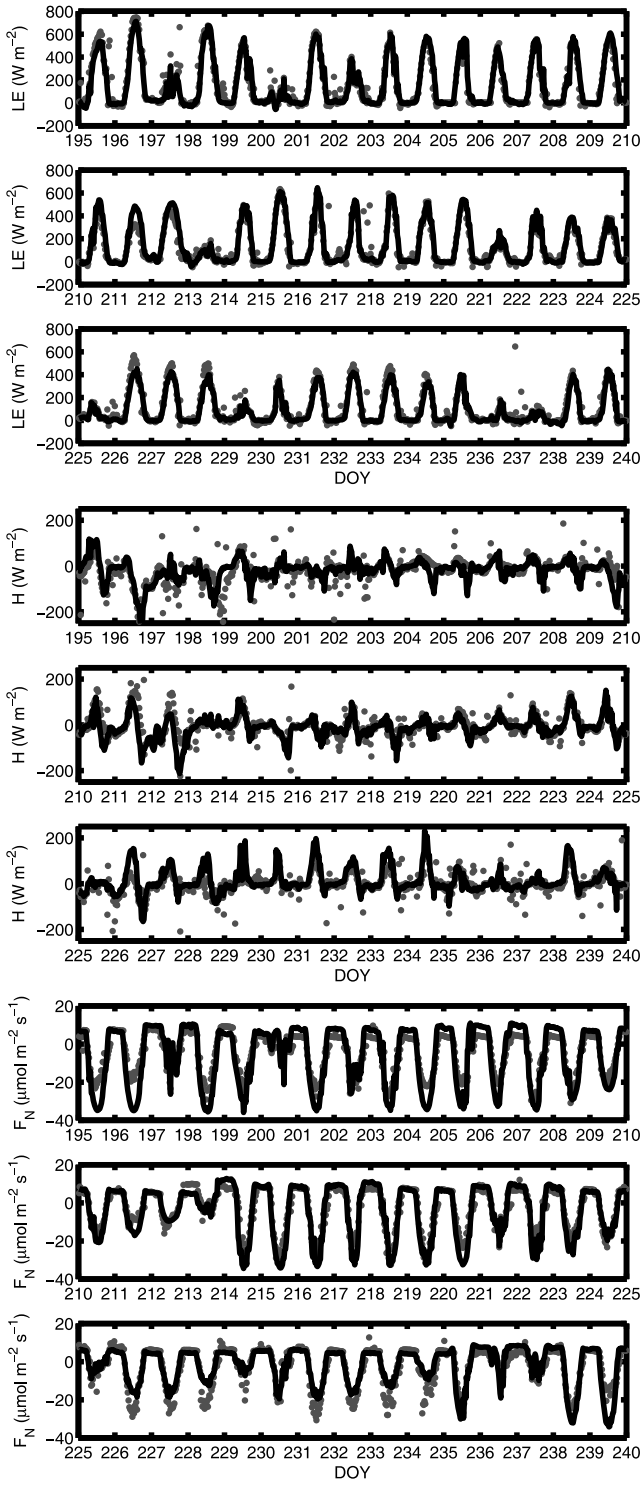

Figure 3. Comparison of the simulated (solid line) and observed (dots) of latent heat flux (*LE*), sensible heat flux (*H*), and net ecosystem CO_2 exchange (F_N).

[23] Our model simulation was restricted to the period from day of year (DOY) 195 to 239. In this period, the canopy was fully closed (LAI > 2). The soil contribution to *H* and *LE*, which was ignored in our model, should be very small. Although not available during the 2006 experiment, subsequent automated chamber observations from this site suggested that soil evaporation was generally less than 10% of ET.

4. Results

4.1. Water, Heat, and CO_2 Fluxes

[24] Here we use the index of agreement (*I*) and root mean square difference (RMSD) to measure the model performance. The index of agreement [*Willmott*, 1981] is defined by

$$I = 1 - \frac{\sum_{i=1}^{N} (p_i - o_i)^2}{\sum_{i=1}^{N} \left(|p_i - \overline{o}| + |o_i - \overline{o}|\right)^2} \quad (1)$$

where p_i and o_i are the predicted and observed values, respectively, for measurement *i*, *N* is the total number of observations, and $\overline{o}$ represents the average value of the observations. An index value of 1 indicates perfect agreement and 0 means no agreement between the simulation and the observation. The root mean square difference RMSD is defined by

$$RMSD = \left[\frac{1}{N}\sum_{i=1}^{N} (p_i - o_i)^2\right]^{1/2} \quad (2)$$

[25] Figure 3 represents the time series of latent and sensible heat fluxes (*LE* and *H*) and net ecosystem CO_2 exchange F_N (positive for CO_2 emission and negative for CO_2 absorption). Here the measured *LE* and *H* were adjusted to achieve perfect energy balance closure. The maximum (minimum) observed value was 748 (−50) W m^{-2}, 196 (−293) W m^{-2} and 33 (−13) μmol m^{-2} s^{-1} for *LE*, *H* and F_N, respectively. The seasonal and diurnal variation was captured by the model, with the index of agreement (*I*) for the *LE*, *H* and F_N simulation equal to 0.97, 0.78 and 0.94 and RMSD of 57 W m^{-2}, 46 W m^{-2} and 6 μmol m^{-2} s^{-1}, respectively.

[26] Obvious biases in the modeled fluxes occurred in two periods, including DOY 209 to 212 and DOY 226 to 235, suggesting that the model breaks down during conditions of water stress. This is common to many models. In the first period, the magnitudes of midday (from 1000 to 1500 LST) *LE* and F_N were overestimated and *H* was underestimated by the model. For example, on the midday of DOY 211, the modeled and observed *LE* was 448 and 305 W m^{-2}, F_N was −15.6 and −8.5 μmol m^{-2} s^{-1} and *H* was 72 and 144 W m^{-2}, respectively. The last significant precipitation event (>31 mm) occurred on DOY 200. Following this event, soil moisture declined steadily to 0.19 m^3 m^{-3} (the lowest of the season) at the 10 cm depth. Even though the highest LAI of ∼8 was recorded on DOY 212, the magnitude of the observed F_N was only 1/3 of that on DOY 215 when PAR was similar but θ was much higher (0.26 m^3 m^{-3}) following precipitation events with amount of 39 and 47 mm on DOY 213 and 214, respectively. In the second period, the magnitude of the *LE* and F_N were underestimated and *H* was overestimated by the model. In this period, θ was very low ranging from 0.19 to

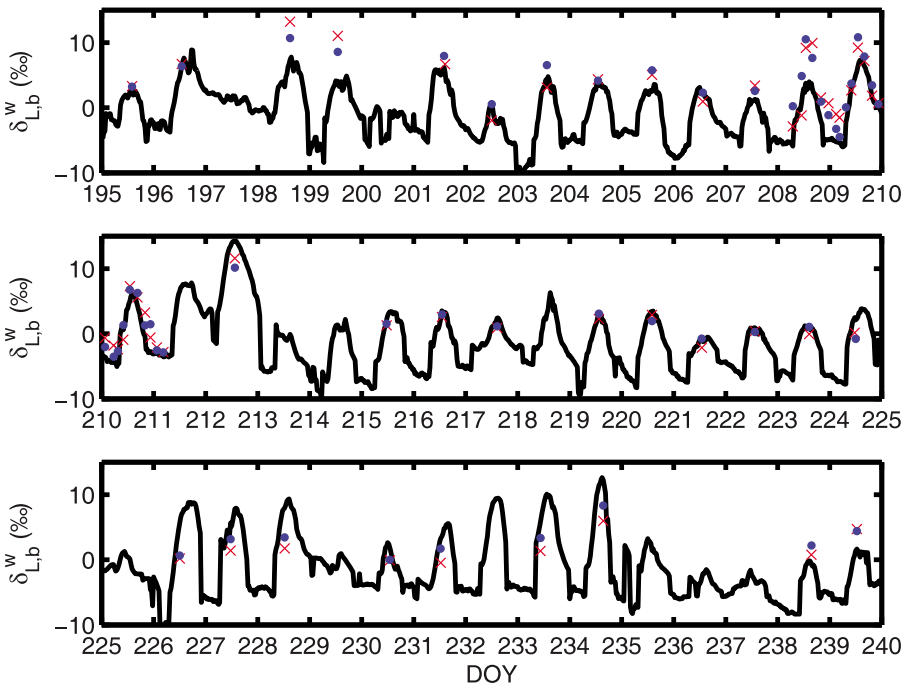

Figure 4. Time series of the simulated (solid line) and observed (crosses, lower canopy; dots, upper canopy) ^{18}O-H_2O composition of the bulk leaf water ($\delta^w_{L,b}$).

0.21 m^3 m^{-3}. The high sensitivity of the soybean system to soil moisture, as indicated by the measurements, was not adequately captured by the model. A better parameterization of the photosynthetic response to the root zone soil moisture is needed to improve the modeled results.

4.2. The ^{18}O Composition of Leaf Water and Evapotranspiration

[27] Figure 4 shows the modeled and observed time series of the isotopic composition of the bulk leaf water ($\delta^w_{L,b}$). The index of agreement was 0.78 and RMSD was 2.9‰ for the midday isotopic composition. The observed mean midday $\delta^w_{L,b}$ value ranged from −2.9 to 13.2‰ for bottom leaves and from −4.5 to 10.8‰ for top leaves, and the modeled values ranged from −1.0 to 14.2‰. The midday $\delta^w_{L,b}$ was underestimated by the model on most days before DOY 212, and overestimated from DOY 224 to 234. Reasonable agreement was achieved between DOY 215 to 223. During the intensive experimental period (from DOY 208 to 210), the diurnal variation was captured by the model although the magnitude of $\delta^w_{L,b}$ variations was underestimated.

[28] Figure 5 reveals the impact of the steady state assumption and the choice of L_{eff} on the prediction of leaf water ^{18}O. Here $\delta^w_{L,b}$ is the average of the upper and lower canopy values. Nonsteady state (dots) improved the simulation slightly, with $R^2 = 0.39$ ($N = 39$), compared to steady state simulation (Figure 5a, pluses) with $R^2 = 0.33$. The marginal improvement confirms that nonsteady state effects were small near midday when the measurement was made. Simulation using a typical value of 15 mm for L_{eff} found in the literature introduced an obvious bias (crosses), with $R^2 = 0.22$. In the scatterplot of the predictions for $\delta^w_{L,e}$ in nonsteady state and in steady state (Figure 5b), most data points deviated from the 1:1 line except during some nighttime periods when dew events occurred. During the dew events, both predictions gave identical results. Figure 5c presents the diurnal composite of the deviation between the two predictions (nonsteady state value minus steady state $\delta^w_{L,e}$ value). From 0730 to 1430 LST, the deviation was negative with the most negative value of −0.6 ‰ occurring around 1030 LST, which indicates that δ^w_{ET} was lower than that of source (xylem) water δ^w_x δ^w_x and ^{18}O-H_2O was accumulating in the leaf water. Over the time period from 1500 to 0700 LST, the deviation was positive with the maximum value of 1.3‰ occurring at 1900 LST, which indicates that δ^w_{ET} was greater than δ^w_x.

[29] Figure 6 shows the diurnal composite of the modeled and observed δ^w_{ET}. The reader is reminded that SiLSM ignored the soil evaporation contribution to ET, which is expected to have a small influence when LAI > 2 and would act to lower δ^w_{ET}. Both composites include periods influenced by nighttime dew events. In the whole study period, δ^w_x ranged from −5.5‰ to −8.4‰, with a mean value of −7.4‰. During the daytime (from 0800 to 1800 LST), the modeled δ^w_{ET} ranged from −9.6 to −4.3‰, and the observed value ranged from −7.3 to −2.8‰. The simulated and observed δ^w_{ET} reached their daily peak value 11.6 ‰ and 6.9‰, respectively, at almost the same time in the evening (around 2000 LST). From 1830 to 0730 LST, the observed δ^w_{ET} was noisy and reached a minimum value of −24.9‰, while the simulated δ^w_{ET} did not get lower than −9.6‰. The deviation of the observed and modeled δ^w_{ET} from δ^w_x provides strong evidence for nonsteady state of the leaf water isotopic exchange.

[30] Figure 6 shows that the Farquhar and Cernusak model, when scaled to the whole canopy, captured reasonably well the temporal dynamics of δ^w_{ET} in the dew-free period (1000–1800 LST). In the hours between 1900 and 0900 LST, the δ^w_{ET} observation was confounded by the influence of dew formation which occurred around 80% of the nights between DOY 195 and 239. The performance of their model was inadequate during these periods.

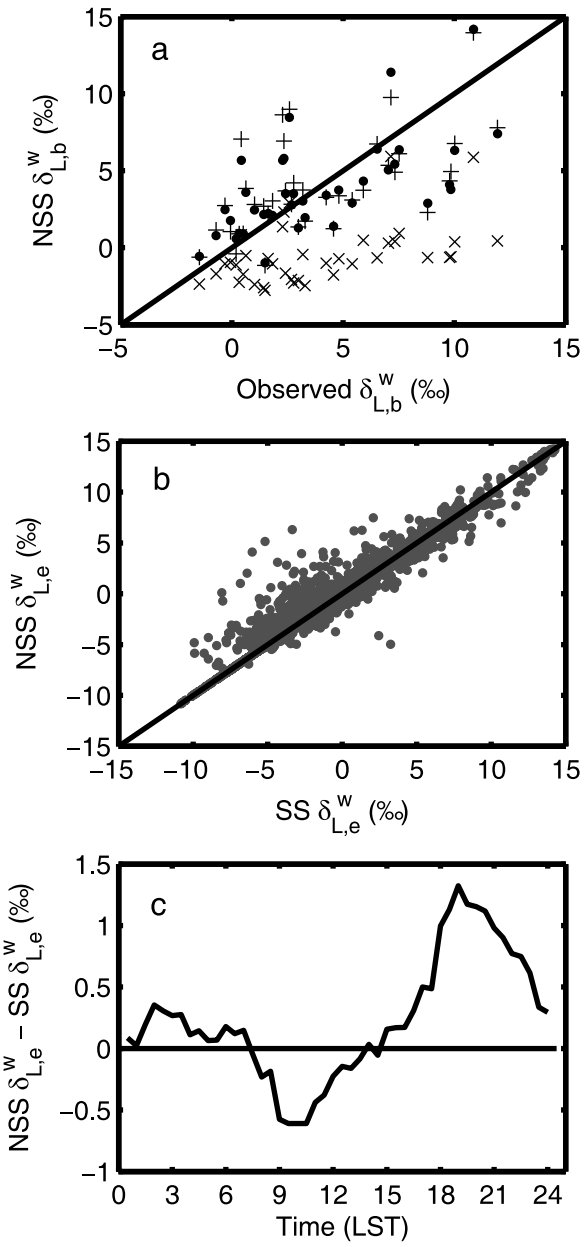

Figure 5. Comparison of the ^{18}O-H_2O composition of leaf water. (a) Prediction of $\delta^w_{L,b}$ versus the observed $\delta^w_{L,b}$ (dots, NSS prediction; pluses, SS prediction; crosses, NSS prediction with $L_{\text{eff}} = 15$ mm); (b) NSS versus SS prediction of $\delta^w_{L,e}$; (c) diurnal composite variations of the difference between NSS and SS prediction of $\delta^w_{L,e}$.

4.3. The ^{18}O-CO_2 Isoforcing

[31] Figure 7 shows the time series of the modeled and observed eddy isoforcing both in good fetch and poor fetch conditions. The seasonal and diurnal variation was captured by SiLSM, with the index of agreement (I) between all the observation and those model results at the corresponding time of 0.81, and RMSD of 142 μmol m^{-2} s^{-1} ‰ ($N = 1522$).

[32] Figure 8 shows the 24 h composite of the modeled partition of the ecosystem eddy ^{18}O-CO_2 isoforcing C_a ($w'\delta'$). The net isoforcing was positive in the daytime, which acted to enrich the atmosphere with ^{18}O-CO_2, and negative at night causing the depletion of ^{18}O-CO_2. The canopy component dominated the isoforcing in the daytime, with a peak value of 355 μmol m^{-2} s^{-1} ‰ at 1430 LST, and was negligible at night. The soil component was negative, ranging from −70 to −37 μmol m^{-2} s^{-1} ‰.

[33] Both the model simulation and the observation indicate that the ^{18}O-CO_2 exchange was strongly influenced by relative humidity (in reference to canopy temperature, Figure 9). The observed relationship can be expressed by the linear regression $y = 470 - 6.2x$ with $R^2 = 0.45$. The model data for the same periods can be described by a linear regression with roughly the same slope but different intercept ($y = 760 - 8.3x$, $R^2 = 0.71$). The offset between the modeled and observed relationships was mostly likely a model bias (see also Figure 8).

4.4. Sensitivity Analyses

[34] Three sets of sensitivity analysis were performed, including sensitivity to unconstrained model parameters, to the way processes was handled in the model, and to driving variables (Table 1). The first set concerns the impact of the two unconstrained model parameters, CO_2 hydration efficiency in the leaves (θ_{eq}) and in soil ($\theta_{eq,s}$). We found that θ_{eq} had a significant effect on the eddy CO_2 isoforcing. The default value of 0.75 was employed in SiLSM [*Gillon and Yakir*, 2000]. If we change it to 0.5 (a relative change of −33%) or 1.0 (+33%), the diurnal peak value of the eddy isoforcing changes to 175 (−39%) and 396 μmol m^{-2} s^{-1} ‰ (+39%), respectively (Table 1 and Figure 10). Very small changes in the nighttime simulation were detected (Figure 10), with the minimum value of −44 and −48 μmol mol m^{-2} s^{-1} ‰ for θ_{eq} of 0.5 and 1, respectively, in comparison of −46 μmol m^{-2} s^{-1} ‰ corresponding to the default θ_{eq}. The above result agrees with the sensitivity analysis of *Riley et al.* [2002, 2003] suggesting that lowering θ_{eq} results in less daytime ecosystem CO_2 flux enrichment to the atmosphere and little effect at night. The sensitivity to θ_{eq} may have been the primary cause of the model overprediction

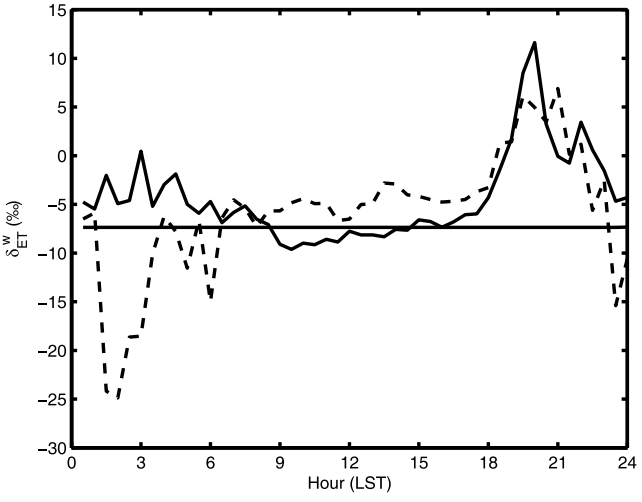

Figure 6. Diurnal composite of ^{18}O-H_2O composition of simulated (solid line) and measured (dashed line) evapotranspiration δ^w_{ET}. The straight solid line is the seasonal mean δ^w_x.

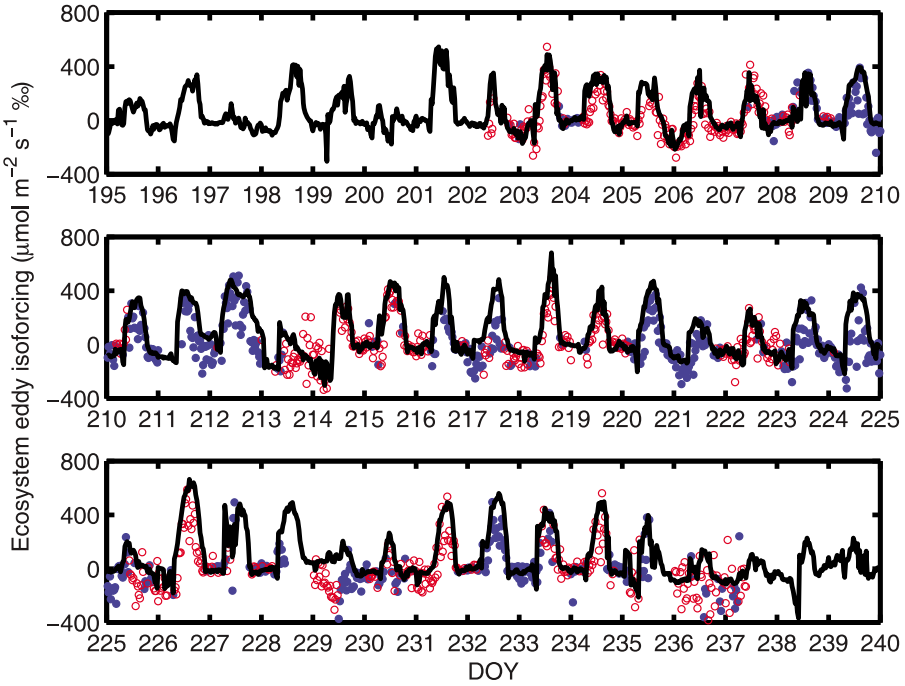

Figure 7. Time series of the ecosystem eddy ^{18}O-CO_2 isoforcing (solid line, simulation; circles, observations with poor fetch; dots, observations with good fetch).

of the ecosystem isoforcing (Figures 7, 8, and 10 and section 5.3).

[35] The default value of 1.0 was employed for $\theta_{eq,s}$ in SiLSM. If we lower it to 0.5, the ecosystem eddy isoforcing increased to 330 μmol m^{-2} s^{-1} ‰ for daily peak value (a relative change of 16%) and to −18 μmol m^{-2} s^{-1} ‰ for minimum value (Figure 10).

[36] The second set of analyses deals with how the key exchange processes are handled in the SiLSM submodels. In the LSM submodel, the adjusted *LE* and *H* measurements were used for parameter optimization. If the original measurement without adjustment for energy balance closure was used instead, the coefficients in the soil moisture function (equation (C15)) b_1 and b_2 would change to −5.4 and 19.3 from −5.8 and 24.9 for θ below 0.21 and to −1.0 and −1.5 from −1.5 and 0.5 for θ higher than 0.21, respectively. The two parameters in the stomatal function D_0 and a_1 changed to 0.32 kPa and 8.1 from 0.44 and 16.2, respectively. The diurnal peak value of the eddy ^{18}O-CO_2 isoforcing decreased to 279 μmol m^{-2} s^{-1} ‰ (a relative change of −2%) and the minimum value at night increased to −40 μmol m^{-2}s^{-1} ‰. The 24 h mean value increased by 18%.

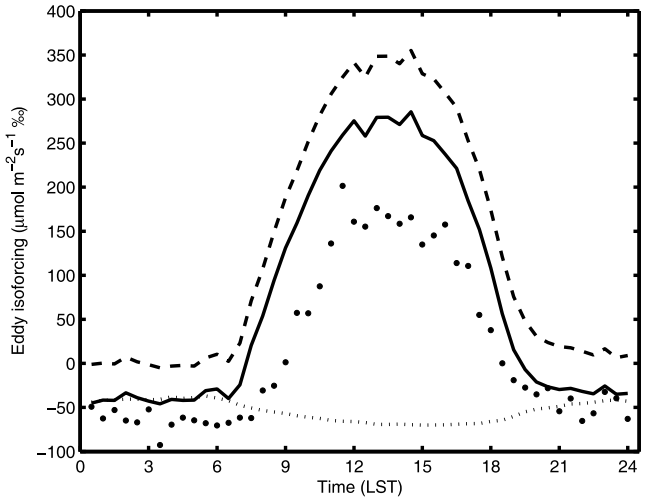

Figure 8. Diurnal composite of the eddy ^{18}O-CO_2 isoforcing (solid line, simulated ecosystem eddy isoforcing; dashed line, simulated canopy eddy isoforcing; dotted line, simulated soil eddy isoforcing; dots, observation).

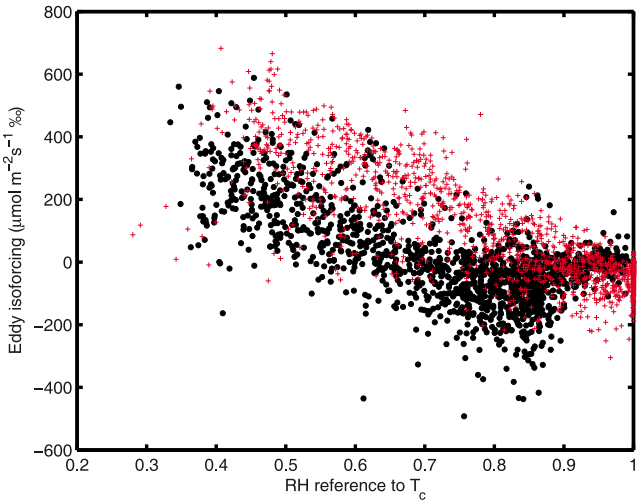

Figure 9. The relationship between ecosystem isoforcing and relative humidity referenced to canopy temperature. Dots, measurement; pluses, simulation.

Table 1. Sensitivity Analysis of the Modeled Diurnal Peak Value of C_a ($\overline{w'\delta'}$)[a]

	Changes	Diurnal Peak Value of C_a ($\overline{w'\delta'}$) (μmol m^{-2} s^{-1} ‰)	Sensitivity (%)
Parameters			
θ_{eq}	−0.25 (absolute)	175	−39
	+0.25 (absolute)	396	+39
$\theta_{eq,s}$	−0.5 (absolute)	330	+16
Processes	without forcing energy balance	279	−2
	calculating $\delta_{L,e}$ in steady state	289	+1
	ignoring turbulent diffusion	575	+102
Driving variables			
C_a	+100% (relative)	681	+139
RH	+2% (absolute)	242	−15
T_a	+1 K (absolute)	288	+1
u_m	−10% (relative)	264	−7
h	−50% (relative)	205	−28
θ	−10% (relative)	265	−7
δ_s^w	+2‰ (absolute)	305	+7
	−2‰ (absolute)	266	−7

[a]For reference, the modeled diurnal peak value with default parameters is 285 μmol m^{-2}s^{-1} ‰. The observed peak value is 201 μmol m^{-2} s^{-1} ‰.

[37] In the $H_2^{18}O$ submodel, assuming steady state caused the daily peak value of eddy ^{18}O-CO_2 isoforcing to increase slightly to 289 μmol m^{-2} s^{-1} ‰ (+ 1%) and shifted the peak time earlier by 1.5 h, consistent with the difference between steady versus nonsteady state prediction of $\delta_{L,e}^w$ (Figure 5c). Even though the peak eddy isoforcing value did not change much, ignoring the nonsteady state can cause errors in the timing of the predicted eddy isoforcing.

[38] In the isoforcing submodel, turbulence diffusion had a significant effect on the eddy isoforcing. Ignoring turbulent diffusion in the kinetic effects by dropping aerodynamic resistance r_a from equations (A8), (A9), and (B4), increased the daily peak eddy isoforcing to 575 μmol m^{-2} s^{-1} ‰, or a relative change of +102%, substantially worsening the comparison with the measured values.

[39] The third set of analyses aims to quantify the sensitivity of the isoforcing to the observed driving variables of the model. For example, a doubling of C_a increased the diurnal peak value of C_a ($\overline{w'\delta'}$) to 681 μmol m^{-2} s^{-1} ‰ (+139%), although in terms of isoforcing $\overline{w'\delta'}$, the increase was minor, from 0.019 to 0.023 ‰ m s^{-1} (+21%) (more on this point in section 5.4). *Lee et al.* [2009] showed that $\overline{w'\delta'}$, not C_a ($\overline{w'\delta'}$), is the appropriate flux boundary condition for calculating the atmospheric budget of ^{18}O-CO_2. Additional information on the isoforcing sensitivity can be found in Table 1.

5. Discussion

5.1. Effect of Energy Imbalance on Model Simulations

[40] The lack of energy balance closure in the eddy covariance measurements introduces an important problem in the LSM model validation [*Wilson et al.*, 2002]. Since LSM models are based on the principle of energy budget conservation, optimization against the measured flux time series may lead to erroneous parameters for calculating *LE*, *H* and F_N. For example, by training the parameters D_0, a_1, b_1 and b_2 to optimize the fit of *LE*, we found that the predicted *H* was biased high in comparison to the (unadjusted) observed values. This is because to satisfy energy conservation, the model was forced to assign the missing energy to *H*. Assuming that the Bowen ratio, as defined by the eddy covariance measurement of *H* and *LE,* and the available energy were accurately measured, we trained the LSM model using the adjusted *H* and *LE*. This method seems logical. Similar conclusions can be found in the study of *Aranibar et al.* [2006]. Forcing energy balance closure can therefore improve the LSM model performance.

[41] The effect of energy balance closure on the isotopic flux prediction is less straightforward. In comparison to the original model results with forced energy balance closure, the diurnal peak eddy isoforcing, simulated with the LSM model optimized against the unadjusted flux measurement, was 2% lower (Table 1). The apparent small sensitivity was a result of two opposing processes. On the one hand, if the LSM was trained against the original *H* and *LE* measurement, the midday (from 1000 to 1500 LST) predicted *H* increased to an average of 127 W m^{-2} in comparison to the default prediction of 29 W m^{-2}, the midday *LE* decreased to 264 W m^{-2} in comparison to the original 372 W m^{-2}, and the midday predicted canopy temperature T_c was on average 301.6 K in comparison to the original 299.9 K, over the simulation

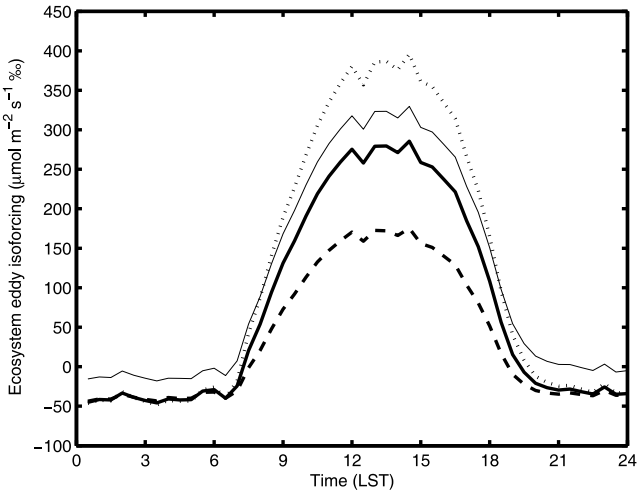

Figure 10. Effect of CO_2 hydration extent (θ_{eq} and $\theta_{eq,s}$) on the eddy CO_2 isoforcing calculation. Solid line, θ_{eq} = 0.75 and $\theta_{eq,s}$ = 1 (default); dashed line, θ_{eq} = 0.5 and $\theta_{eq,s}$ = 1; dotted line, θ_{eq} = 1.0 and $\theta_{eq,s}$ = 1; thin solid line, θ_{eq} = 0.75 and $\theta_{eq,s}$ = 0.5.

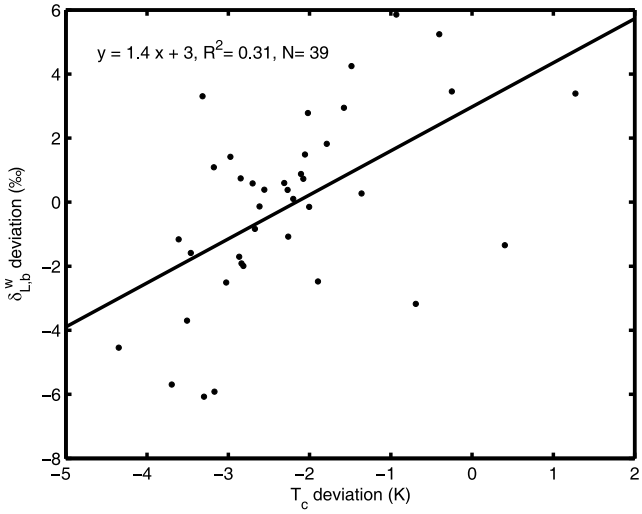

Figure 11. Relationship between model errors in $\delta^w_{L,b}$ and T_c, with $R^2 = 0.31$. Solid line is a best fit regression with the equation shown.

period (DOY 195–239). A higher T_c would mean a lower relative humidity RH_i and therefore a higher $\delta^w_{L,e}$, $\delta^c_{L,e}$ and $^{18}O\text{-}CO_2$ isoforcing (Figures 7 and 8). The reduction in *LE* was linked to a larger canopy resistance, which acted to increase the kinetic factors (ε^c_k and ε^w_k). Both an increased $\delta^c_{L,e}$ and increased canopy kinetic factors resulted in an increase in the magnitude of terms in the square brackets of equation (A2), and tended to increase the eddy isoforcing. On the other hand, the canopy CO_2 flux F_c changed to -23 μmol $m^{-2}s^{-1}$ in comparison to the original -24 μmol m^{-2} s^{-1}. In the daytime, $F_c < 0$ and $C_c - C_a < 0$ because of photosynthesis, a less negative F_c would offset the isoforcing enhancement due to $\delta^c_{L,e}$ and ε^c_k.

5.2. The $^{18}O\text{-}H_2O$ Exchange

[42] Our results suggest that nonsteady effects may be more important than the Péclet effect in controlling δ^w_{ET}. Optimization of the Farquhar and Cernusak model resulted in a vanishingly small radial diffusion length (equation (B9)) or the Péclet number. In other words, the Dongmann's approximation that $\delta^w_{L,e} = \delta^w_{L,b}$ was acceptable at the canopy scale in the present study [*Dongmann et al.*, 1974]. The same approximation was also found to give reasonable prediction of δ^w_{ET} over a forest ecosystem [*Lee et al.*, 2007]. The negligibly small Péclet effect may be an emergent property at the ecosystem scale. In the physical space of a canopy, transpiration occurs at numerous sites, the leaves, that are dispersed throughout a fragmented media. So true diffusion does not exist at the canopy scale because liquid water molecules cannot move across these isolated transpiration sites.

[43] The accuracy of the SiLSM $^{18}O\text{-}H_2O$ calculations also depends on factors that are external to the $^{18}O\text{-}H_2O$ submodel. For example, we found that the prediction error in $\delta^w_{L,b}$ was correlated with the error in T_c (Figure 11). On most days before DOY 212, $\delta^w_{L,b}$ was underestimated by SiLSM, when H and T_c were underestimated and RH_i was overestimated. From DOY 224 to 234, the simulated H was higher than the observation, and $\delta^w_{L,b}$ was overestimated (Figures 4 and 5).

5.3. Extent of CO_2 Hydration

[44] The extent of CO_2 hydration (θ_{eq}) in the leaves and the canopy kinetic fractionation (ε_k) were the two most crucial factors controlling the $^{18}O\text{-}CO_2$ flux according to the sensitivity analysis (Table 1). If turbulence was ignored in the kinetic factors, the simulated eddy isoforcing was much too high in comparison to the observation. But even with accounting for turbulent diffusion, the simulated eddy isoforcing was still biased high (Figures 7 and 8). The sensitivity analysis suggests that the default θ_{eq} of 0.75 was likely too high. This value was adopted from *Gillon and Yakir* [2000], who calculated the CO_2 hydration extent from in-vitro CA activity and gas exchange by adapting the equation developed by *Mills and Urey* [1940]. *Cousins et al.* [2006] showed that θ_{eq} derived from $C^{18}OO$ discrimination measurements is sensitive to irradiance. They found that in field conditions, θ_{eq} of the wild-type *Flaveria bidentis* changed from 1.06 in low radiation (PAR = 150 μmol m^{-2} s^{-1}) to 0.45 in high radiation (PAR = 2000 μmol m^{-2} s^{-1}). Our analyses also suggest that the extent of CO_2 hydration should be much lower for plants growing in field conditions than the value derived from the CA activity and photosynthetic flux measurement: Optimization against the eddy isoforcing observed in midday periods yielded a value of 0.46 for θ_{eq}.

[45] Three alternative explanations exist for the disagreement shown in Figures 7 and 8, but none of them seems plausible. First, the predicted $\delta^w_{L,e}$ may have been biased high. However, forcing a good agreement for the eddy isoforcing would require that the midday $\delta^w_{L,e}$ be 1.6‰ lower than the observed $\delta^w_{L,b}$, which is an unacceptable result.

[46] Second, the estimate of the soil isoforcing component could be in error because it assumes that soil CO_2 was in equilibrium with soil water at a single depth of 10 cm. In reality, soil CO_2 flux originates from multiple layers. For example, *Jacinthe and Lal* [2009] found that around 81% of soil respiration comes from the 0 to 20 cm soil layer in a soybean field and the remaining contributed by deeper soil. Over the period DOY 195 to 239, the 10 cm soil water δ^w_s was 1.5 per mil higher than that of the root zone average [*Welp et al.*, 2008]. If the latter value was used for the soil isoforcing calculation, the peak ecosystem isoforcing would be lower by less than 7% (Table 1), and not enough to explain the discrepancy in Figure 8. Furthermore, the discrepancy would be even larger if a value less than 1 were used for $\theta_{eq,s}$ (Table 1 and Figure 10).

[47] The third explanation is related to uncertainties in the isoforcing measurement. The eddy isoforcing data, obtained from the first attempt at measuring the ecosystem-scale isotopic fluxes with eddy covariance, was very noisy (Figure 7). The noise, however, appears to be random. One could suppose that the 31% deficit in the energy budget implies a similar amount of bias of the isoforcing measurement. If an adjustment of this size was made, the disagreement between the model and the observation would largely vanish. However, no mechanisms are known to cause identical biases in the eddy covariance measurement of energy fluxes (sensible and latent heat) and in those of passive scalars such as CO_2 and its isotopes [*Baldocchi*, 2003; *Huang et al.*, 2008]. An

independent estimate of the eddy isoforcing based on the gradient-diffusion theory shows good agreement with the eddy covariance measurement, indicating that a large systematic bias in the latter was unlikely (L. R. Welp et al., manuscript in preparation, 2010). We are, therefore, left with a low hydration efficiency at the most logical explanation for the disagreement shown in Figures 7 and 8.

5.4. Implication of Elevated CO_2 Concentration, Humidity, and Temperature

[48] In the interest of understanding how the isoforcing may change in a future CO_2-enriched world, the sensitivity test with CO_2 concentration deserves additional scrutiny. The results show that the isoforcing $w'\delta'$ is moderately sensitive to CO_2, increasing by 19% in response to a doubling of the observed CO_2 level. In CO_2-enriched conditions, plants tend to increase their photosynthesis and reduced transpiration via increasing the stomatal resistance [*Anderson et al.*, 2001; *Drake et al.*, 1997; *Long et al.*, 2004; *Maherali et al.*, 2002, 2003]. In our 2 × CO_2 sensitivity test, the magnitude of the canopy CO_2 flux (F_c) increased by 17% (from −24 to −28 μmol m^{-2} s^{-1}, mean values for periods 1000 to 1500 LST), *LE* decreased by 19% (from 372 to 300 W m^{-2}) and the stomatal resistance (r_s^w) increased by 94% (from 1.05 to 2.04 m^2 s mol^{-1}). The small change in isoforcing $w'\delta'$ was a result of several opposing mechanisms. The increase of r_s^w and reduction of r_a (due to air being more unstable) increased the kinetic fractionation factor for ^{18}O-H_2O ε_k^w by 5.4‰, $\delta_{L,e}^w$ by 2.9‰ and the kinetic factor for ^{18}O-CO_2 ε_k^c by 1.3‰, in the midday periods, all acting to increase the canopy isoforcing according to equation (A2). Similarly, the increase in F_c magnitude should also enhance the isoforcing. However, increased C_a had the opposite effect, acting to reduce the isoforcing through a reduction in the magnitude of the concentration ratio $C_c/(C_c - C_a)$ in equation (A2).

[49] The isotopic fractionation processes may also respond to increasing atmospheric humidity. Our observational and modeling results show that relative humidity was an important driver on the short-term (hourly) variations in the ^{18}O-CO_2 isoforcing (Figure 10). The model sensitivity analysis revealed that a 2% absolute change in the air relative humidity (RH) would cause a 15% reduction in the daytime peak isoforcing (Table 1), primarily through the reduction in $\delta_{L,b}^w$ (by 1.3‰). The $\delta_{L,b}^w$ sensitivity (−0.7 per mil change per 1% absolute increase in air relative humidity) was higher than the Craig-Gordon model prediction [*Still et al.*, 2009] in part because of the reduction in canopy temperature in high-humidity conditions, which further amplified the humidity effect on $\delta_{L,b}^w$. The significant negative correlation between RH and $\delta_{L,b}^w$ have been reported in the literature [*Welp et al.*, 2008]. Some of the humidity effect may be offset by the concurrent rise in air temperature although the temperature sensitivity appears very small (Table 1). It is not known whether the documented rise in humidity [*Willett et al.*, 2007; *Santer et al.*, 2007; *Dai*, 2006] can cause a measureable reduction in the global mean ^{18}O composition of atmospheric CO_2.

6. Conclusions

[50] The diagnostic analysis using SiLSM suggests that the Péclet effect played a much less important role than the nonsteady effect on the ^{18}O-H_2O exchange in the soybean ecosystem. In the LSM modeling framework, the accuracy of the prediction of the foliage ^{18}O-H_2O enrichment depended critically on the accuracy of the canopy temperature calculation and on the proper handling of turbulent diffusion in the kinetic fractionation process.

[51] The modeled results demonstrate that in agreement with the observation, relative humidity exerted a large influence on the short-term (hourly) ^{18}O-CO_2 exchange between the ecosystem and the atmosphere. The SiLSM prediction of the ^{18}O-CO_2 isoforcing was 49% higher than the observed midday mean value. Forcing agreement of the predicted with the observed isoforcing yielded a value of 0.46 for θ_{eq}, suggesting a low hydration efficiency in the leaves of soybean in field conditions.

[52] Atmospheric humidity is likely to increase in a future CO_2-enriched world. Our model sensitivity analysis revealed that a 2% absolute change in the air relative humidity would cause a 15% reduction in the daytime peak isoforcing. Some of the humidity effect may be offset by the effect of the rise in CO_2. It is not known whether the documented rise in humidity [*Willett et al.*, 2007; *Santer et al.*, 2007; *Dai*, 2006] can cause a measureable reduction in the global mean ^{18}O composition of atmospheric CO_2.

Appendix A: Big-Leaf Parameterization for ^{18}O-CO_2 Isoforcing

[53] *Lee et al.* [2009] showed that the covariance between the vertical velocity and isotope composition in delta notation ($\overline{w'\delta'}$) is the eddy flux of δ. Physically, this covariance term represents the surface boundary condition for the atmospheric budget of δ and can be parameterized through the big-leaf analogy. The total covariance consists of a canopy $(\overline{w'\delta'})_c$ and a soil $(\overline{w'\delta'})_s$ component,

$$\overline{w'\delta'} = \left(\overline{w'\delta'}\right)_c + \left(\overline{w'\delta'}\right)_s \tag{A1}$$

$$\left(\overline{w'\delta'}\right)_c = \frac{F_c}{C_a}\left[\frac{C_c}{C_c - C_a}\left(\delta_{L,e}^c - \delta_a^c\right)\theta_{eq} + \left(1-\theta_{eq}\right)\varepsilon_k^c\frac{C_c}{C_a} - \varepsilon_k^c\right] \tag{A2}$$

$$\left(\overline{w'\delta'}\right)_s = \frac{F_s}{C_a}\left[\frac{C_s}{C_s - C_a}\left(\delta_s^c - \delta_a^c\right)\theta_{eq,s} + \left(1-\theta_{eq,s}\right)\varepsilon_{k,s}^c\frac{C_s}{C_a} - \varepsilon_{k,s}^c\right] \tag{A3}$$

where F_c and F_s are the canopy and soil components of the net ecosystem CO_2 exchange calculated by the LSM model, δ_a^c is the ^{18}O-CO_2 composition of the ambient air, $\delta_{L,e}^c$ and δ_s^c are ^{18}O compositions of CO_2 in the stomatal cavity and the soil pore space and in full equilibrium with the leaf and soil laminar water, respectively, ε_k^c and $\varepsilon_{k,s}^c$ are canopy and soil kinetic fractionation factors for ^{18}O-CO_2. The CO_2 hydration extent in the leaves (θ_{eq}) was assigned a value of 0.75 for the soybean ecosystem [*Gillon and Yakir*, 2000], and that in the soil ($\theta_{eq,s}$) was set to 1. In the present study, the simulated average daytime minimum C_i was 1.3 × 10^4 μmol m^{-3} (296 ppm), C_c was 1.1 × 10^4 μmol m^{-3} (269 ppm) and C_s

was 2.4×10^4 μmol m^{-3} (567 ppm) and the observed daytime minimum C_a at the reference height was 1.5×10^4 μmol m^{-3} (357 ppm).

[54] The CO_2 concentration in the chloroplasts of the leaves (C_c) and soil air (C_s) are calculated from

$$C_c = C_a + F_c\left(r_a + r_b^c + r_s^c + r_m^c\right) \tag{A4}$$

$$C_s = C_a + F_s\left(r_a + r_{a,c} + r_{soil}^c\right) \tag{A5}$$

where C_a is the atmospheric CO_2 concentration, r_a and $r_{a,c}$ are aerodynamic resistance from canopy top to the reference height and that from soil surface to canopy top, r_b^c, r_m^c, r_s^c and r_{soil}^c are canopy-scale boundary layer, mesophyll, stomatal and soil resistances to CO_2.

[55] According to [*Brenninkmeier et al.*, 1983], $\delta_{L,e}^c$ and δ_s^c are given by

$$\delta_{L,e}^c = \delta_{L,e}^w + \frac{17604}{T_c} - 17.93 \tag{A6}$$

$$\delta_s^c = \delta_s^w + \frac{17604}{T_s} - 17.93 \tag{A7}$$

where $\delta_{L,e}^w$ and δ_s^w are ^{18}O-H_2O composition at the evaporating site in the leaf and that in the soil at the 10 cm depth, respectively, T_s and T_c are soil temperature at 10 cm depth and canopy temperature.

[56] The canopy kinetic fractionation factor for ^{18}O-CO_2 (ε_k^c) are given by

$$\varepsilon_k^c = \frac{5.8r_b^c + 8.8r_s^c + 0.8r_m^c}{r_a + r_b^c + r_s^c + r_m^c}\left(‰\right) \tag{A8}$$

where the coefficient 0.8 represents the mesophyll fractionation factor [*Farquhar and Lloyd*, 1993].

[57] The soil kinetic fractionation factor for ^{18}O-CO_2 $\varepsilon_{k,s}^c$ is given by

$$\varepsilon_{k,s}^c = \frac{8.8r_{soil}^c}{r_a + r_{a,c} + r_{soil}^c}\left(‰\right) \tag{A9}$$

Appendix B: Equations for Nonsteady State ^{18}O-H_2O Composition of Leaf Water

[58] Accounting for the change in the water content and the Péclet effect, *Farquhar and Cernusak* [2005] describe the ^{18}O-H_2O at the evaporating site in the nonsteady state ($\delta_{L,e}^w$) as

$$\delta_{L,e}^w = \delta_{L,es}^w - \frac{\alpha_k^w \alpha_{eq}^w r_c^w}{w_i} \cdot \frac{d\left(W \cdot \frac{1-e^{-P}}{P} \cdot \left(\delta_{L,e}^w - \delta_x^w\right)\right)}{dt} \tag{B1}$$

where r_c^w is the canopy resistance to diffusion of water vapor to the atmosphere from the sites of evaporation within the leaf including stomata resistance r_s^w and boundary layer resistance r_b^w in series, δ_x^w is ^{18}O-H_2O composition of xylem water, and t is time. The equilibrium fractionation factor α_{eq}^w (>1) is given by *Majoube* [1971], and

$$\varepsilon_{eq}^w = \left(1 - \frac{1}{\alpha_{eq}^w}\right) \times 1000\left(‰\right) \tag{B2}$$

[59] The kinetic fractionation factor for water vapor diffusion α_k^w (>1) is calculated as,

$$\alpha_k^w = 1 + \frac{\varepsilon_k^w}{1000} \tag{B3}$$

$$\varepsilon_k^w = \frac{21r_b^w + 32r_s^w}{r_a + r_b^w + r_s^w}\left(‰\right) \tag{B4}$$

[60] The water content in the foliage, W is expressed as mass of water per unit ground area (g m^{-2}). In the paper of *Farquhar and Cernusak* [2005], equation (B1) is based on the principle of ^{18}O-H_2O mass conservation of leaf water. Here we applied it to the canopy scale. To be consistent with the canopy scale application, W is computed as the product of LAI and the leaf water content measured in the field. The Péclet number P is related to transpiration rate (E) via:

$$P = \frac{EL_{eff}}{CD} \tag{B5}$$

where C is the density of liquid water (55.5×10^3 mol m^{-3}), D is the diffusivity of ^{18}O-H_2O in water depending on temperature [*Cuntz et al.*, 2007], L_{eff} is the scaled effective "radial" length from the evaporative site.

[61] In equation (B1), $\delta_{L,es}^w$ is the isotopic enrichment of water at the evaporating site in steady state,

$$\delta_{L,es}^w = (R_{es}/R_{VSMOW} - 1) \times 1000\left(‰\right) \tag{B6}$$

$$\frac{R_{es}}{R_x} = \alpha_{eq}^w\left[\alpha_k^w(1 - RH_i) + RH_i\frac{R_v}{R_x}\right] \tag{B7}$$

where R_v, R_x and R_{es} are $^{18}O/^{16}O$ in ambient vapor, xylem water and leaf water at the evaporative site in steady state, respectively, RH_i is relative humidity in fraction in reference to the canopy temperature, and R_{VSMOW} is the standard $^{18}O/^{16}O$ ratio of the Vienna Standard Mean Ocean Water (VSMOW).

[62] In this paper, $\delta_{L,e}^w$ was used to determine the isotope exchange between CO_2 and H_2O. However, $\delta_{L,e}^w$ is not directly observable. For the purpose of model verification, the predicted ^{18}O-H_2O composition of evapotranspiration δ_{ET}^w and of the bulk leaf water ($\delta_{L,b}^w$) were compared with the measurements. Here, δ_{ET}^w and $\delta_{L,b}^w$ were calculated according to the departure from steady state as

$$\delta_{ET}^w = \frac{\delta_{L,e}^w - \delta_{L,es}^w}{\alpha_k^w \alpha_{eq}^w(1 - RH_i)} + \delta_x^w \tag{B8}$$

and

$$\delta^w_{L,b} = \delta^w_{L,bs} - \frac{\alpha_k \alpha_{eq} r^w_t}{w_i} \cdot \frac{1 - e^{-P}}{P} \cdot \frac{d\left(W \cdot \left(\delta^w_{L,b} - \delta^w_x\right)\right)}{dt} \quad \text{(B9)}$$

where $\delta^w_{L,bs}$ is δ^{18}O-H_2O of bulk leaf water in steady state and calculated from $\delta^w_{L,e}$ and P as

$$\delta^w_{L,bs} = \frac{\delta^w_{L,es}(1 - e^{-P})}{P} \quad \text{(B10)}$$

[63] Equations (B1) and (B9) were solved iteratively by finding a zero difference between the left and right-hand sides of each equation. Usually 30 to 40 steps of iteration were needed for each time step of SiLSM to reach a preset zero threshold.

[64] Dew events were considered explicitly because of their frequent occurrence (around 80% of nights) [*Welp et al.*, 2008]. In our model, r^w_s was set to zero during dew events, and the ^{18}O-H_2O compositions of the leaf water at the site of evaporation ($\delta^w_{L,e}$) and evapotranspiration water (δ^w_{ET}) were assumed to equilibrate with that of water vapor in ambient air (δ^w_a) as

$$\delta^w_{ET} = \delta^w_a + \varepsilon^w_{eq} \quad \text{(B11)}$$

$$\delta^w_{L,e} = \delta^w_a + \varepsilon^w_{eq} \quad \text{(B12)}$$

Appendix C: Big-Leaf Land Surface Model

C1. Water, Heat, and CO_2 Fluxes

[65] In the LSM the bulk exchange relation is used to calculate the sensible and latent heat flux densities [*Beljaars and Holtslag*, 1991], in conjunction with the energy budget equation

$$(1 - \alpha)R_S + \varepsilon R_L - \varepsilon \sigma T_c^4 = H + LE + G \quad \text{(C1)}$$

where R_S and R_L are incoming short-wave and long-wave radiation flux, H is sensible heat flux, LE is latent heat flux, G is soil heat flux, ε is surface emissivity, α is canopy surface albedo, σ is the Stefan-Boltzmann constant and T_c is canopy surface or skin temperature. The sensible and latent heat fluxes are given by

$$H = \frac{\rho_a c_p (T_c - T_a)}{r_a} \quad \text{(C2)}$$

$$LE = \rho_a \lambda \frac{q*(T_c) - q_a}{r_a + r^w_s} \quad \text{(C3)}$$

where ρ_a is air density, c_p is isobaric specific heat, T_a is air temperature at reference height, λ is latent heat of vaporization, $q^*(T_c)$ is saturation specific humidity at canopy surface, q_a is specific humidity at reference height. Canopy temperature (T_c) is solved from a linearized form of equation (C1).

[66] The canopy CO_2 flux is calculated as

$$F_c = \frac{C_i - C_a}{r_a + r^c_s + r^c_b} \quad \text{(C4)}$$

[67] To get the stomatal resistances r^w_s and r^c_s, an analytic formulation based on radiation transfer within the canopy is used to upscale the leaf stomatal conductance g^c_l to the canopy conductance g^c_c [*Ronda et al.*, 2001].

[68] At leaf scale, the stomatal conductance is solved from the plant physiological approach as

$$g^c_l = g_{\min,c} + \frac{a_1 A_g}{(C_l - \Gamma)\left(1 + \frac{D_s}{D_0}\right)} \quad \text{(C5)}$$

where A_g is the gross assimilation rate, $g_{\min,c}$ is the cuticular conductance, C_l is the CO_2 concentration at the leaf surface, D_s is the vapor pressure deficit at plant level, D_0 and a_1 are empirical parameters.

[69] The gross assimilation rate is computed as a function of T_c, photosynthetically active radiation (PAR) and the intercellular CO_2 concentration (C_i) [*Jacobs*, 1994].

$$A_g = (A_m + R_d)\left\{1 - e^{-[\alpha PAR/(A_m + R_d)]}\right\} \quad \text{(C6)}$$

with

$$A_m = A_{m,\max}\{1 - e^{-\left[g_m(C_i - \Gamma)/A_{m,\max}\right]}\} \quad \text{(C7)}$$

where α is the light use efficiency [*Collatz et al.*, 1991, 1992], $A_{m,\max}$ is the maximal primary productivity under high light conditions and high CO_2 concentrations, g_m is the mesophyll conductance for CO_2, Γ is the CO_2 compensation point, which are functions of the canopy temperature [*Jacobs*, 1994]. The scheme described by *Collatz et al.* [1991, 1992] and *Jacobs* [1994] is used to compute g^c_m, C_i and $A_{m,\max}$.

[70] The dark respiration R_d is calculated as

$$R_d = 0.11 A_m \quad \text{(C8)}$$

[71] The effect of soil moisture on net photosynthesis and canopy conductance is accounted for by relating the gross assimilation rate to soil moisture in the root zone so that the water-stressed gross assimilation rate is expressed as

$$A_g = A^*_g f(\theta) \quad \text{(C9)}$$

where A_g* is the unstressed rate, and $f(\theta)$ is a function of soil moisture (see below).

C2. Resistance Terms

[72] The canopy-scale stomatal resistance to CO_2 r^c_s is the inverse of g^c_c, and the stomatal resistance to H_2O r^w_s is calculated from

$$r^w_s = r^c_s / 1.6 \quad \text{(C10)}$$

[73] The canopy-scale mesophyll resistance to CO_2 r_m^c is calculated as

$$r_m^c = 1/\left(g_m^c \times LAI\right) \tag{C11}$$

[74] The canopy-scale boundary layer resistance to H_2O r_b^w, aerodynamic resistance r_a and the aerodynamic resistance from the soil surface to the canopy top $r_{a,c}$ are computed using the methods described by *Lee et al.* [2009].

[75] Soil resistance for H_2O is calculated from soil moisture [*Sellers et al.*, 1992],

$$r_{soil}^w = \exp(8.206 - 4.225 \times \theta)\ \left(\mathrm{s\ m^{-1}}\right) \tag{C12}$$

[76] The resistance terms to CO_2 are given by

$$r_{soil}^c = 1.6 r_{soil}^w \tag{C13}$$

$$r_b^c = 1.4 r_b^w \tag{C14}$$

C3. Major Changes to the Big-Leaf LSM

[77] Three important changes are made to the big-leaf LSM. First, a logistic expression for the soil moisture effect is used instead of the original quadratic one since our optimization analyses show that the original formulation does not work well under very dry soil conditions,

$$f(\theta) = 1/(1 + \exp(-b_1 - b_2\beta(\theta))) \tag{C15}$$

with $\beta(\theta)$ given by

$$\beta(\theta) = \max\left[0, \min\left(1, \frac{\theta - WP}{FC - WP}\right)\right] \tag{C16}$$

where FC and WP are the soil moisture content at field capacity and at permanent wilting point, respectively, and b_1 and b_2 are empirical coefficients determined in the above analysis. The soil moisture content at 10 cm depth (θ) is expressed as a volume fraction.

[78] Second, the original LSM does not consider soil respiration (F_s). Here, F_s is expressed as a function of soil temperature measured at 10 cm depth (T_s) according to the total nighttime ecosystem respiration measured with eddy covariance,

$$F_s = (-0.19\exp(0.003(T_s - 273.15))) \times 0.81 \tag{C17}$$

where the factor 0.81 acknowledges that 81% of ecosystem respiration is soil respiration according to the soil chamber and eddy covariance observations for the soybean field [*Bavin et al.*, 2009].

[79] The original LSM does not consider dew formation. At this site, dew was a common phenomenon at night. We consider dew formation in the evening and the subsequent evaporation of the dew water in the morning in the energy budget calculation. The dew formation routine is activated whenever the dew point of canopy air exceeded the surface skin temperature. When a dew event occurs, the stomatal resistance to H_2O (r_s^w) is set to zero in the energy budget calculation. Dew forms at the rate of water vapor flux determined from the energy budget calculation. Once RH_i reduces to a value lower than 1, the dew water would evaporate at the rate of the predicted water vapor flux. Leaf transpiration would turn on after all the dew that formed in the previous evening had evaporated.

Notation

$()^c$	CO_2.
$()^w$	H_2O.
α	albedo, dimensionless.
α	light use efficiency, mg J^{-1}.
α_{eq}^w	equilibrium fractionation factor for water (>1), dimensionless.
α_k^w	kinetic fractionation factor for water vapor (>1), dimensionless.
Γ	CO_2 compensation point, mg m^{-3}.
δ_a^c	δ^{18}O-CO_2 of air at height z_m, ‰.
δ_s^c	δ^{18}O-CO_2 of soil air, ‰.
$\delta_{L,e}^c$	δ^{18}O- CO_2 in equilibrium with water at leaf evaporative site, ‰.
δ_a^w	δ^{18}O-H_2O of water vapor at reference height z_m, ‰.
δ_{ET}^w	δ^{18}O-H_2O of evapotranspiration, ‰.
$\delta_{L,b}^w$	δ^{18}O-H_2O of bulk leaf water, ‰.
$\delta_{L,bs}^w$	steady state value of $\delta_{L,b}^w$, ‰.
$\delta_{L,e}^w$	δ^{18}O-H_2O at evaporative site in leaf, ‰.
$\delta_{L,es}^w$	steady state values of $\delta_{L,e}^w$, ‰.
δ_s^w	δ^{18}O-H_2O of soil water, ‰.
δ_x^w	δ^{18}O-H_2O of xylem water, ‰.
ε_k^c	canopy kinetic fractionation factor for ^{18}O-CO_2, ‰.
$\varepsilon_{k,s}^c$	soil kinetic fractionation factor for ^{18}O-CO_2, ‰.
ε_{eq}^w	equilibrium ^{18}O fractionation between liquid water and vapor, ‰.
ε_k^w	canopy kinetic fractionation factor for ^{18}O-H_2O, ‰.
θ	volumetric soil moisture content at 10 cm depth.
θ_{eq}	extent of CO_2 hydration in leaves, equal to 0.75.
$\theta_{eq,s}$	extent of CO_2 hydration in soil, equal to 1.
$\overline{w'\delta'}$	whole-ecosystem (kinematic) isoforcing, ‰ m s^{-1}.
$C_a\ (\overline{w'\delta'})$	ecosystem eddy ^{18}O-CO_2 isoforcing, μmol m^{-2} s^{-1} ‰.
A_g	gross assimilation rate, mg m^{-2} s^{-1}.
A_m	primary productivity, mg m^{-2} s^{-1}.
a_1	empirical coefficient in the canopy resistance model, equal to 16.2.
b_1	empirical coefficient for soil moisture stress, equal to −5.8 for $\theta \le 0.21$, −1.5 for $\theta > 0.21$.
b_2	empirical coefficient for soil moisture stress, equal to −24.9 for $\theta \le 0.21$, 0.5 for $\theta > 0.21$.
C	molar concentration of water, equal to 55.5×10^3 mol m^{-3}.
C_a	CO_2 molar concentration of the air at height z_m, μmol m^{-3}.
C_c	CO_2 molar concentration in leaf chloroplasts, μmol m^{-3}.

C_i CO_2 molar concentration in the intercellular space, μmol m^{-3}.
C_l CO_2 concentration at the leaf surface, μmol m^{-3}.
C_s CO_2 molar concentration in soil air, μmol m^{-3}.
D diffusivity of ^{18}O-H_2O in water, m^2 s^{-1}.
D_0 vapor pressure deficit constant, equal to 0.44 kPa.
D_s vapor pressure deficit at plant level, kPa.
E transpiration rate, mol m^{-2} s^{-1}.
FC volumetric soil moisture content at field capacity, equal to 0.36.
F_c canopy CO_2 flux, μmol m^{-2} s^{-1}.
F_s soil CO_2 flux, μmol m^{-2} s^{-1}.
F_N net ecosystem CO_2 flux, μmol m^{-2} s^{-1}.
g_c^c canopy-scale stomatal conductance, m s^{-1} or mol m^{-2} s^{-1}.
g_l^c leaf-scale stomatal conductance, m s^{-1} or mol m^{-2} s^{-1}.
g_m^c leaf-scale mesophyll conductance, m s^{-1} or mol m^{-2} s^{-1}.
g_{min}^c leaf-scale cuticular conductance for CO_2, m s^{-1} or mol m^{-2} s^{-1}.
h canopy height, m.
H sensible heat flux density, W m^{-2}.
L_{eff} scaled effective "radial" length, m.
LE latent heat flux, W m^{-2}.
P Péclet number, dimensionless.
q_a specific humidity at reference height z_m, g g^{-1}.
$q^*(T_c)$ saturation specific humidity at canopy temperature, g g^{-1}.
r_a aerodynamic resistance in the surface layer, s m^{-1} or m^2 s mol^{-1}.
$r_{a,c}$ aerodynamic resistance in the canopy air layer, s m^{-1} or m^2 s mol^{-1}.
r_b canopy-scale boundary layer resistance, s m^{-1} or m^2 s mol^{-1}.
r_m^c canopy-scale mesophyll resistance to CO_2, s m^{-1} or m^2 s mol^{-1}.
r_s canopy-scale stomatal resistance, s m^{-1} or m^2 s mol^{-1}.
r_{soil} soil resistance, s m^{-1} or m^2s mol^{-1}.
r_t^w canopy-scale total resistance to water vapor and heat from canopy surface to reference height, s m^{-1} or m^2 s mol^{-1}.
R_{es} $^{18}O/^{16}O$ in leaf water at the evaporative site in steady state, dimensionless.
R_v $^{18}O/^{16}O$ of water vapor in ambient air, dimensionless.
R_x $^{18}O/^{16}O$ of xylem water, dimensionless.
R_L incoming longwave radiation flux density, W m^{-2}.
R_S incoming shortwave radiation flux density, W m^{-2}.
RH_i relative humidity of the ambient air reference to T_c (fraction).
T_a air temperature at the reference level, K.
T_c canopy temperature, K.
T_s soil temperature at 10 cm depth, K.
w_i mole fraction of (light) water vapor in the intercellular spaces, mol mol^{-1}.
W leaf water content (mass of water per unit ground area at the canopy scale), g m^{-2}.
WP volumetric soil moisture content at permanent wilting point, equal to 0.18.

[80] **Acknowledgments.** This research was supported by the Chinese Academy of Sciences International Partnership Project (grant CXTD-Z2005-1 to X.L. and Q.Y.), the U.S. National Science Foundation through grants DEB-0514904 (to X.L.) and DEB-0514908 and ATM-0546476 (to T.G.), and a Rice Family Foundation grant (to X.L.). The first author also acknowledges a visiting doctoral fellowship from the State Scholarship Fund of China.

References

Anderson, L. J., et al. (2001), Gas exchange and photosynthetic acclimation over subambient to elevated CO_2 in a C_3-C_4 grassland, *Global Change Biol.*, *7*, 693–707, doi:10.1046/j.1354-1013.2001.00438.x.

Aranibar, J. N., et al. (2006), Combining meteorology, eddy fluxes, isotope measurements, and modeling to understand environmental controls of carbon isotope discrimination at the canopy scale, *Global Change Biol.*, *12*, 710–730, doi:10.1111/j.1365-2486.2006.01121.x.

Baker, J. M., and T. J. Griffis (2005), Examining strategies to improve the carbon balance of corn/soybean agriculture using eddy covariance and mass balance techniques, *Agric. For. Meteorol.*, *128*, 163–177, doi:10.1016/j.agrformet.2004.11.005.

Baldocchi, D. D. (2003), Assessing the eddy covariance technique for evaluating carbon dioxide exchange rates of ecosystems: Past, present and future, *Global Change Biol.*, *9*, 479–492, doi:10.1046/j.1365-2486.2003.00629.x.

Baldocchi, D. D., and D. R. Bowling (2003), Modelling the discrimination of $^{13}CO_2$ above and within a temperate broad-leaved forest canopy on hourly to seasonal time scales, *Plant Cell Environ.*, *26*, 231–244, doi:10.1046/j.1365-3040.2003.00953.x.

Barbour, M. M., and G. D. Farquhar (2000), Relative humidity- and ABA-induced variation in carbon and oxygen isotope ratios of cotton leaves, *Plant Cell Environ.*, *23*, 473–485, doi:10.1046/j.1365-3040.2000.00575.x.

Barbour, M. M., et al. (2000), Variation in the oxygen isotope ratio of phloem sap sucrose from Castor Bean. Evidence in support of the Péclet Effect, *Plant Physiol.*, *123*, 671–679, doi:10.1104/pp.123.2.671.

Bavin, T. K., et al. (2009), Impact of reduced tillage and cover cropping on the greenhouse gas budget of a maize/soybean rotation agricultural ecosystem, *Agric. Ecosyst. Environ.*, *134*, 234–242, doi:10.1016/j.agee.2009.07.005.

Beljaars, A. C. M., and A. A. M. Holtslag (1991), Flux parameterization over land surfaces for atmospheric models, *J. Appl. Meteorol.*, *30*, 327–341, doi:10.1175/1520-0450(1991)030<0327:FPOLSF>2.0.CO;2.

Bender, M., et al. (1994), The Dole effect and its variations during the last 130000 years as measured in the Vostok ice core, *Global Biogeochem. Cycles*, *8*, 363–376, doi:10.1029/94GB00724.

Blanken, P. D., et al. (1997), Energy balance and canopy conductance of a boreal Aspen forest: Partitioning overstory and understory components, *J. Geophys. Res.*, *102*, 28,915–28,927, doi:10.1029/97JD00193.

Brenninkmeier, C., et al. (1983), Oxygen isotope fractionation between CO_2 and H_2O, *Isot. Geosci.*, *1*, 181–190.

Cernusak, L. A., et al. (2002), Diurnal variation in the stable isotope composition of water and dry matter in fruiting Lupinus angustifolius under field conditions, *Plant Cell Environ.*, *25*, 893–907, doi:10.1046/j.1365-3040.2002.00875.x.

Cernusak, L. A., et al. (2003), Oxygen isotope composition of phloem sap in relation to leaf water in *Ricinus communis*, *Funct. Plant Biol.*, *30*, 1059–1070, doi:10.1071/FP03137.

Cernusak, L. A., et al. (2005), Environmental and physiological controls over oxygen and carbon isotope composition of Tasmanian blue gum, *Eucalyptus globulus*, *Tree Physiol.*, *25*, 129–146.

Ciais, P., et al. (1997), A three-dimensional synthesis study of $\delta^{18}O$ in atmospheric CO_2: 1. Surface fluxes, *J. Geophys. Res.*, *102*, 5857–5872, doi:10.1029/96JD02360.

Collatz, G. J., et al. (1991), Physiological and environmental regulation of stomatal conductance, photosynthesis and transpiration: A model that includes a laminar boundary layer, *Agric. For. Meteorol.*, *54*, 107–136, doi:10.1016/0168-1923(91)90002-8.

Collatz, G. J., et al. (1992), Coupled photosynthesis-stomatal conductance model for leaves of C_4 plants, *Aust. J. Plant Physiol.*, *19*, 519–538, doi:10.1071/PP9920519.

Cousins, A. B., et al. (2006), A transgenic approach to understanding the influence of carbonic anhydrase on $C^{18}OO$ discrimination during C_4 photosynthesis, *Plant Physiol.*, *142*, 662–672, doi:10.1104/pp.106.085167.

Cullen, L. E., et al. (2008), Analyses of $\delta^{13}C$ and $\delta^{18}O$ in tree rings of *Callitris columellaris* provide evidence of a change in stomatal control of

photosynthesis in response to regional changes in climate, *Tree Physiol.*, *28*, 1525–1533.
Cuntz, M., et al. (2003a), A comprehensive global three-dimensional model of $\delta^{18}O$ in atmospheric CO_2: 1. Validation of surface processes, *J. Geophys. Res.*, *108*(D17), 4527, doi:10.1029/2002JD003153.
Cuntz, M., et al. (2003b), A comprehensive global three-dimensional model of $\delta^{18}O$ in atmospheric CO_2: 2. Mapping the atmospheric signal, *J. Geophys. Res.*, *108*(D17), 4528, doi:10.1029/2002JD003154.
Cuntz, M., et al. (2007), Modelling advection and diffusion of water isotopologues in leaves, *Plant Cell Environ.*, *30*, 892–909, doi:10.1111/j.1365-3040.2007.01676.x.
Dai, A. (2006), Recent climatology, variability, and trends in global surface humidity, *J. Clim.*, *19*, 3589–3606, doi:10.1175/JCLI3816.1.
Dongmann, G., et al. (1974), On the enrichment of $H_2^{18}O$ in the leaves of transpiring plants, *Radiat. Environ. Biophys.*, *11*, 41–52, doi:10.1007/BF01323099.
Drake, B. G., et al. (1997), More efficient plants: A consequence of rising atmospheric CO_2?, *Annu. Rev. Plant Physiol. Plant Mol. Biol.*, *48*, 609–639, doi:10.1146/annurev.arplant.48.1.609.
Epstein, S., and C. Yapp (1977), Isotope tree thermometers, *Nature*, *266*, 477–478, doi:10.1038/266477a0.
Farquhar, G. D., and L. A. Cernusak (2005), On the isotopic composition of leaf water in the non-steady state, *Funct. Plant Biol.*, *32*, 293–303, doi:10.1071/FP04232.
Farquhar, G. D., and J. Lloyd (1993), Carbon and oxygen isotope effects in the exchange of carbon dioxide between terrestrial plants and the atmosphere, in *Stable Isotopes and Plant Carbon-Water Relations*, edited by J. R. Ehleringer et al., pp. 47–70, Academic, San Diego, Calif.
Farquhar, G. D., et al. (1993), Vegetation effects on the isotope composition of oxygen in atmospheric CO_2, *Nature*, *363*, 439–443, doi:10.1038/363439a0.
Flanagan, L. B., et al. (1991), Comparison of modeled and observed environmental influences on the stable oxygen and hydrogen isotope composition of leaf water in *Phaseolus vulgaris* L, *Plant Physiol.*, *96*, 588–596, doi:10.1104/pp.96.2.588.
Flanagan, L. B., et al. (1994), Effect of changes in leaf water oxygen isotopic composition on discrimination against $CO^{18}O^{16}$ during photosynthetic gas exchange, *Aust. J. Plant Physiol.*, *21*, 221–234, doi:10.1071/PP9940221.
Foken, T. (2008), The energy balance closure problem: An overview, *Ecol. Appl.*, *18*(6), 1351–1367, doi:10.1890/06-0922.1.
Gillon, J. S., and D. Yakir (2000), Internal conductance to CO_2 diffusion and $C^{18}OO$ discrimination in C_3 leaves, *Plant Physiol.*, *123*, 201–213, doi:10.1104/pp.123.1.201.
Gillon, J., and D. Yakir (2001), Influence of carbonic anhydrase activity in terrestrial vegetation on the ^{18}O content of atmospheric CO_2, *Science*, *291*, 2584–2587, doi:10.1126/science.1056374.
Gray, J., and P. Thompson (1976), Climatic information from $^{18}O/^{16}O$ ratios of cellulose in tree rings, *Nature*, *262*, 481–482, doi:10.1038/262481a0.
Griffis, T. J., et al. (2005a), Seasonal dynamics and partitioning of isotopic CO_2 exchange in a C_3/C_4 managed ecosystem, *Agric. For. Meteorol.*, *132*, 1–19, doi:10.1016/j.agrformet.2005.06.005.
Griffis, T. J., et al. (2005b), Feasibility of quantifying ecosystem-atmosphere $C^{18}O^{16}O$ exchange using laser spectroscopy and the flux-gradient method, *Agric. For. Meteorol.*, *135*, 44–60, doi:10.1016/j.agrformet.2005.10.002.
Griffis, T. J., et al. (2007), Determining carbon isotope signatures from micrometeorological measurements: Implications for studying biosphere-atmosphere exchange processes, *Boundary Layer Meteorol.*, *123*, 295–316, doi:10.1007/s10546-10006-19143-10548.
Griffis, T. J., et al. (2008), Direct measurement of biosphere-atmosphere isotopic CO_2 exchange using the eddy covariance technique, *J. Geophys. Res.*, *113*, D08304, doi:10.1029/2007JD009297.
Harwood, K. G., et al. (1998), Diurnal variation of $\Delta^{13}CO2$, $\Delta C^{18}O^{16}O$ and evaporative site enrichment of $\delta H_2^{18}O$ in *Piper aduncum* under field conditions in Trinidad, *Plant Cell Environ.*, *21*, 269–283, doi:10.1046/j.1365-3040.1998.00276.x.
Hoffmann, G., et al. (2004), A model of the Earth's Dole effect, *Global Biogeochem. Cycles*, *18*, GB1008, doi:10.1029/2003GB002059.
Huang, J., et al. (2008), A modelling study of flux imbalance and the influence of entrainment in the convective boundary layer, *Boundary Layer Meteorol.*, *127*, 273–292, doi:10.1007/s10546-007-9254-x.
Jacinthe, P., and R. Lal (2009), Tillage effects on carbon sequestration and microbial biomass in reclaimed farmland soils of southwestern Indiana, *Soil Sci. Soc. Am. J.*, *73*(2), 605–613, doi:10.2136/sssaj2008.0156.
Jacobs, C. M. J. (1994), Direct impact of atmospheric CO_2 enrichment on regional transpiration, Ph.D. thesis, 179 pp., Wageningen Agric. Univ., Wageningen, Netherlands.
Lee, X., et al. (2005), In situ measurement of the water vapor $^{18}O/^{16}O$ isotope ratio for atmospheric and ecological applications, *J. Atmos. Oceanic Technol.*, *22*, 555–565, doi:10.1175/JTECH1719.1.
Lee, X., K. Kim, and R. Smith (2007), Temporal variations of the isotopic signal of the whole-canopy transpiration in a temperate forest, *Global Biogeochem. Cycles*, *21*, GB3013, doi:10.1029/2006GB002871.
Lee, X., et al. (2009), Canopy-scale kinetic fractionation of atmospheric carbon dioxide and water vapor isotopes, *Global Biogeochem. Cycles*, *23*, GB1002, doi:10.1029/2008GB003331.
Libby, L. M., et al. (1976), Isotopic tree thermometers, *Nature*, *261*, 284–288, doi:10.1038/261284a0.
Long, S. P., et al. (2004), Rising atmospheric carbon dioxide: Palnt FACE the future, *Annu. Rev. Plant Physiol.*, *55*, 591–628, doi:10.1146/annnurev.arplant.1155.031903.141610.
Maherali, H., et al. (2002), Stomatal acclimation over a subambient to elevated CO_2 gradient in a C_3/C_4 grassland, *Plant Cell Environ.*, *25*, 557–566, doi:10.1046/j.1365-3040.2002.00832.x.
Maherali, H., et al. (2003), Stomatal sensitivity to vapour pressure difference over a subambient to elevated CO_2 gradient in a C_3/C_4 grassland, *Plant Cell Environ.*, *26*, 1297–1306, doi:10.1046/j.1365-3040.2003.01054.x.
Majoube, M. (1971), Oxygen-18 and deuterium fractionation between water and steam, *J. Chim. Phys. Phys. Chim. Biol.*, *68*, 1423–1436.
McDowell, N., et al. (2008), Understanding the stable isotope composition of biosphere-atmosphere CO_2 exchange, *Eos Trans. AGU*, *89*(10), 94–95, doi:10.1029/2008EO100002.
Mills, G. A., and H. C. Urey (1940), The kinetics of isotopic exchange between carbon dioxide, bicarbonate ion, carbonate ion and water, *J. Am. Chem. Soc.*, *62*, 1019–1026, doi:10.1021/ja01862a01010.
Ogee, J., et al. (2004), Partitioning net ecosystem carbon exchange into net assimilation and respiration with canopy-scale isotopic measurements: An error propagation analysis with $^{13}CO_2$ and $CO^{18}O$ data, *Global Biogeochem. Cycles*, *18*, GB2019, doi:10.1029/2003GB002166.
Ogee, J., et al. (2007), Non-steady-state, non-uniform transpiration rate and leaf anatomy effects on the progressive stable isotope enrichment of leaf water along monocot leaves, *Plant Cell Environ.*, *30*, 367–387, doi:10.1111/j.1365-3040.2006.01621.x.
Riley, W. J., et al. (2002), A mechanistic model of $H_2^{18}O$ and $C^{18}OO$ fluxes between ecosystems and the atmosphere: Model description and sensitivity analyses, *Global Biogeochem. Cycles*, *16*(4), 1095, doi:10.1029/2002GB001878.
Riley, W. J., et al. (2003), ^{18}O composition of CO_2 and H_2O ecosystem pools and fluxes in a tallgrass prairie: Simulations and comparisons to measurements, *Global Change Biol.*, *9*, 1567–1581, doi:10.1046/j.1529-8817.2003.00680.x.
Roden, J. S., et al. (2000), A mechanistic model for interpretation of hydrogen and oxygen isotope ratios in tree-ring cellulose, *Geochim. Cosmochim. Acta*, *64*(1), 21–35, doi:10.1016/S0016-7037(99)00195-7.
Ronda, R. J., et al. (2001), Representation of the canopy conductance in modeling the surface energy budget for low vegetation, *J. Appl. Meteorol.*, *40*, 1431–1444, doi:10.1175/1520-0450(2001)040<1431:ROTCCI>2.0.CO;2.
Santer, B. D., et al. (2007), Identification of human-induced changes in atmospheric moisture content, *Proc. Natl. Acad. Sci. U. S. A.*, *104*, 15,248–15,253, doi:10.1073/pnas.0702872104.
Sellers, P. J., et al. (1992), Relations between surface conductance and spectral vegetation indices at intermediate (100 m^2 to 15 km^2) length scales, *J. Geophys. Res.*, *97*(D17), 19,033–19,059.
Still, C. J., et al. (2009), Influence of clouds and diffuse radiation on ecosystem-atmosphere CO_2 and $C^{18}OO$ exchanges, *J. Geophys. Res.*, *114*, G01018, doi:10.1029/2007JG000675.
Wang, X.-F., and D. Yakir (1995), Temporal and spatial variations in the oxygen-18 content of leaf water in different plant species, *Plant Cell Environ.*, *18*, 1377–1385, doi:10.1111/j.1365-3040.1995.tb00198.x.
Wang, Y. P., and R. Leuning (1998), A two-leaf model for canopy conductance, photosynthesis and partitioning of available energy I: Model description and comparison with a multi-layered model, *Agric. For. Meteorol.*, *91*, 89–111, doi:10.1016/S0168-1923(98)00061-6.
Welp, L. R., et al. (2008), $\delta^{18}O$ of water vapor, evapotranspiration and the sites of leaf water evaporation in a soybean canopy, *Plant Cell Environ.*, *31*, 1214–1228, doi:10.1111/j.1365-3040.2008.01826.x.
Willett, K. M., et al. (2007), Attribution of observed surface humidity changes to human influence, *Nature*, *449*, 710–712, doi:10.1038/nature06207.
Willmott, C. J. (1981), On the validation of models, *Phys. Geogr.*, *2*, 184–194.
Wilson, K., et al. (2002), Energy balance closure at FLUXNET sites, *Agric. For. Meteorol.*, *113*, 223–243, doi:10.1016/S0168-1923(02)00109-0.

Yakir, D., and X.-F. Wang (1996), Fluxes of CO_2 and water between terrestrial vegetation and the atmosphere estimated from isotope measurements, *Nature*, *380*, 515–517, doi:10.1038/380515a0.

T. J. Griffis, Department of Soil, Water, and Climate, University of Minnesota, Saint Paul, MN 55108, USA.

K. Kim and X. Lee, School of Forestry and Environmental Studies, Yale University, 21 Sachem St., New Haven, CT 06510, USA. (xuhui.lee@yale.edu)

L. R. Welp, Scripps Institution of Oceanography, University of California, San Diego, La Jolla, CA 92093-0244, USA.

W. Xiao, Key Laboratory of Meteorological Disaster of Ministry of Education, College of Applied Meteorology, Nanjing University of Information Science and Technology, Nanjing, Jiangsu 210044, China.

Q. Yu, Plant Functional Biology and Climate Change Cluster, Department of Environmental Sciences, University of Techology Sydney, PO Box 123, Broadway, NSW 2007, Australia.